AN ABSTRACT OF THE THESIS OF

Byron Tristan Donlevy for the degree of Master of Science

in Chemical Engineering presented on January 14, 1977

Title: Measuring Solids Movement in a Large Particle, Air Fluidized Bed: Two New Methods

Abstract approved: Redacted for Privacy

Two new methods for the determination of solids movement in a fluidized bed have been developed and evaluated in this work. The first method used a deflecting plexiglass rod with strain gages attached to the base which is immersed in the bed of fluidized solids. The probe will yield a continuous output of upward and downward solids fluxes moving past the probe. The output is used in conjunction with rectifying and averaging circuit to yield average upward and downward mass fluxes which are used to calculate solids turnover rates. The second method utilizes ferrite tracer material and immersed inductance coil detectors used in conjunction with a compartmental flow model. The transient tracer curves of the probes are then manipulated to calculate vertical solids turnover rates.

The strain gage probe method found turnover rates for a tube filled bed and a tube free bed which was 1 ft^2 (930 cm^2) in area and 1 ft (30.5 cm) high. Bed solids were 0.96 mm (0.038 inch) silica sand. For the tube free bed, turnover rates ranged from

0.58-1.31 gm/cm^2-sec (1.19-2.68 lb/ft^2-sec), U_o/U_{mf} = 1.3-2.0. For the tube filled bed, turnover rates ranged from 0.31-0.78 gm/cm^2-sec (0.63-1.60 lb/ft^2-sec). The inductance probe could not be used due to poor tracer mixing in the small fluidized bed. The inductance probe has been tested in a 1 m^2 (10.8 ft^2) large particle fluidized bed and works well.

Measuring Solids Movement in a Large Particle, Air Fluidized Bed: Two New Methods

by

Byron Tristan Donlevy

A THESIS

submitted to

Oregon State University

in partial fulfillment of
the requirements for the
degree of

Master of Science
Chemical Engineering

Commencement June 1977

APPROVED:

Redacted for Privacy

Professor of Chemical Engineering

Redacted for Privacy

Head of Department of Chemical Engineering

Redacted for Privacy

Dean of Graduate School

Date thesis is presented January 14, 1977

Typed by Lora Wixom for Byron Tristan Donlevy

ACKNOWLEDGMENT

First I would like to express my thanks to Professor Thomas Fitzgerald: a treasure trove of ideas in electronics, applied mathematics and Chemical Engineering. To Professor Octave Levenspiel: thanks for supplying the initial idea which was responsible for half of this thesis. Thanks to Dr. Hans Dahlke for his advice on the ins and outs of strain gages. And finally, a hearty thank you to Professor Charles E. Wicks for his assistance in many not so little things which came up during my two years at Oregon State University. This work was supported by grant number RP-315-1 from the Electric Power Research Institute.

TABLE OF CONTENTS

TABLE OF CONTENTS (continued)

LIST OF FIGURES

LIST OF FIGURES (continued)

NOMENCLATURE

A	area
c	concentration
C	capacitance or a concentration vector
D_s	solids diffusivity, axial or radial
$\bar{d}_p$	mean particle diameter
D	diameter
f	volume fraction used in the Chang model
f_n	particle numbers distribution density function
f_s	fraction of straingage probe length which is contacted by emulsion solids
f_w	particle weight distribution density function
H	height
I	identity matrix
ID	inside diameter
J_v	vertical solids turnover rate or mass flux
J_h	horizontal solids mass flux
L_m	settled bed height
L_{mf}	bed height at minimum fluidizing conditions
L	denotes an inductor or an inductance
n	rotational frequency of dummy strain gage probe
OD	outside diameter
p_{ij}	fractional input coefficient used in the Chang model
P	matrix of p_{ij} values
q_{ij}	intercompartmental volumetric flowrates used in the Chang model
$\bar{R}$	centroid of dummy strain gage probe

NOMENCLATURE (continued)

R	denotes a resistor or a resistance
t	time
U_{mf}	minimum fluidizing velocity of air
U_o	superficial air velocity (air flow rate/cross sectional area)
V	voltage or volume
$\overline{V}_s$	average solids velocity
W	total mass in a region (associated with the turnover model) or width
x	axial or radial distance
X	mass fraction (associated with the turnover model)

Greek Symbols

ε	change in strain gage resistance due to gage strain
λ	particle numbers distribution density function parameter
ρ_{mf}	packing density of bed solids at minimum fluidizing conditions
ρ_s	bulk density of sand particles
τ	torque acting on strain gage probe beam
$\underline{\Phi}$	mass flux of fluidized solids
$\overline{\Phi}$	upward or downward time averaged mass flux moving past probe j
ω	sinusoidal frequency (radians/sec)

MEASURING SOLIDS MOVEMENT IN A LARGE PARTICLE AIR FLUIDIZED BED: TWO NEW METHODS

I. INTRODUCTION

This thesis has two unique aspects: Investigation of a little studied area of fluidization namely the regime of large particle fluidization and the investigation of two new methods for determination of solids movement in a fluidized bed which haven't been used before. The first method utilizes a probe which directly measures solids mass flux moving past it. The probe consists of a cantilevered plastic probe which has strain gages mounted at its base. The gages measure the strain at the probe base which is caused by the deflection of the probe by frictional or drag forces due to solids moving past the probe. The second method involves the measurement of a transient solid tracer concentration within the bed. Ferrite particles are used as a tracer and their presence is detected by means of a coil inserted in dummy heat exchange tubes whose inductance is changed by the proximity of the ferrite material.

The purpose of this study is to evaluate the performance of the two new methods for the measurement of solids movement. Both methods are in-situ (ie, actually located in the bed while the bed is operating) techniques and they have the potential of being used as independent checks of each other's accuracy for the measurement of solids movement within the fluidized bed.

The strain gage probe technique can yield qualitative information on how the bed is performing. Visual inspection of the probe output

can tell one of the bubble activity near the probe by the amplitude of the upward and downward mass flux values.

Quantitatively, the probe could yield information on vertical solids turnover rates. Net upward and downward mass flux values at a probe can be summed and averaged and used to determine whether there is a convective flow pattern within the bed. This phenomenon has been reported by Davidson (1).

The strain gage probe also has the potential of high temperature use in actual coal combustion fluidized beds. The ferrite tracer - inductance probe detector wouldn't be usable due to the loss of the ferro-magnetic properties of the tracer at temperatures above the Curie temperature of the ferrite.

Likewise, the inductance probe can be used for qualitative information of bed behavior. Bubble frequencies can be estimated by the inductance change of the probe due to the presence of a bubble void passing near the probe. Since the ferrite concentration in the pickup region of the probe is decreased by the proximity of a void, the probe output will briefly drop when a bubble passes by. As a result of the probe being able to detect a bubble, it is also possible to get an approximate idea of how well various regions of the bed are fluidized by the relative frequencies of bubble passages and the amplitude swing of the probe when bubbles pass.

THE LARGE PARTICLE REGIME

Briefly, the most unique characteristic of large particle fluidization is the relationship of gas bubble velocity to the superficial air velocity of the air moving up through the solid particles in the bed emulsion or dense phase. For small particle fluidization ($d_p <$ 0.5 mm (0.020 inch)) or the fast bubble regime, the bubble rise velocity through the emulsion phase is greater than the air velocity moving around the solids in the emulsion phase. As the bubble is rising upward, there is a vortex of circulating air moving around the bubble which is known as the bubble cloud. See figure below.

For the large particle regime ($\bar{d}_p \geq$ 0.5 mm (0.020 inch)) the fluidizing air finds it easier to percolate up through the solids than to go up through the emulsion as a bubble. When a bubble does rise in this regime, the bubble rise velocity is less than the gas velocity in the emulsion phase. For this regime, there is a small vortex which circulates only about the bubble equator and the rest of the bubble serves as a short circuit for the air moving through the emulsion phase. See figure below.

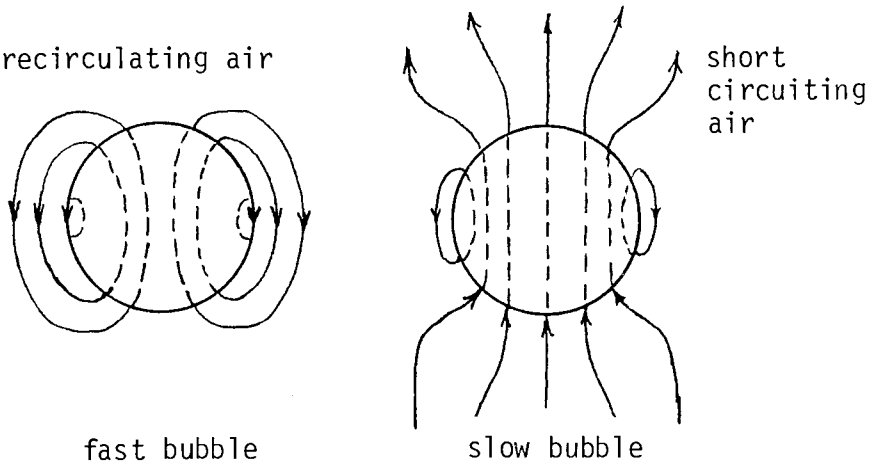

WHY STUDY THE LARGE PARTICLE REGIME AND SOLIDS MOVEMENT?

The regime of large particle fluidization plays a role in the design of a new generation of coal fired power boilers. This new generation of boilers entails two major ideas:

High sulfur content coal and limestone ($CaCO_3$) will be fluidized together while the coal is reacting with the fluidizing air. The limestone, which will be the major component of the bed, will react with the sulfur dioxide (SO_2) to produce calcium sulfate ($CaSO_4$) or gypsum. The gypsum can be removed without extensive wet scrubbing of the stack gas which was previously necessary for the SO_2 removal. The limestone and coal particles will be on the order of 6 mm (0.25) inch) or larger which is in the large particle or slow bubble regime.

The use of heat exchange tubes immersed in the burning fluidized bed to extract heat for steam generation is also a new idea. It is not presently known what effect these tubes will have on the movement of solids within the bed. If there is inhibition of solids movement due to the presence of tubes in the burning bed, there may be hot spots or coal starved regions within the bed due to poor mixing of solids. The nearly isothermal behavior of a properly operating fluidized bed was one of the reasons for choosing such a bed for a boiler and it would be undesirable to unknowingly design a tube array in the bed which would cause non-isothermal behavior.

SUMMARY OF THE MECHANISMS OF FLUIDIZED BED SOLIDS MOVEMENT

Solids are conveyed upward through the bed as a result of the upward passage of a gas bubble. There are believed to be two transport mechanisms. The first way is to be carried upward in the wake of the bubble. The wake is a small turbulent region of solids located on the underside of the bubble. The solids are held in place by air rushing into the underside of the bubble. The bubble will carry the wake up to the surface of the bed where the bubble will burst and leave behind the wake solids on the top of the bed. See the figure below.

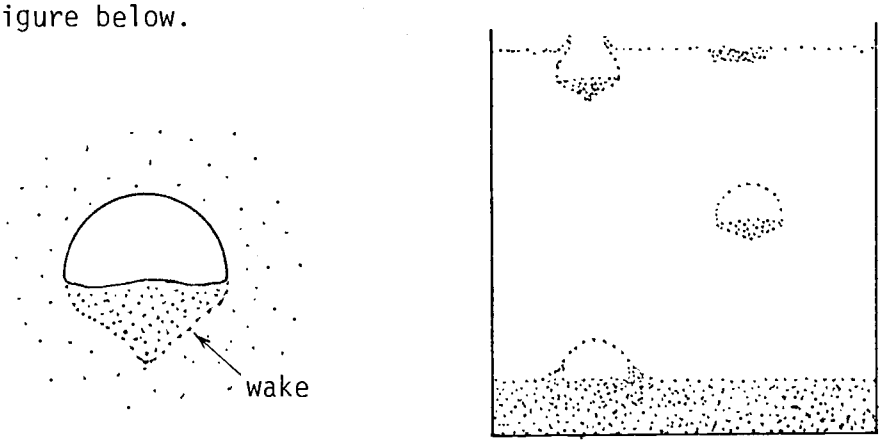

The second method for solids vertical displacement is known as drift induced motion. This type of movement is unrelated to the bubble wake. Potential flow theory for a rising bubble in any type of fluid predicts the drift motion. The movement is caused by the solids or fluid being pushed aside by the rising bubble. See the figure below.

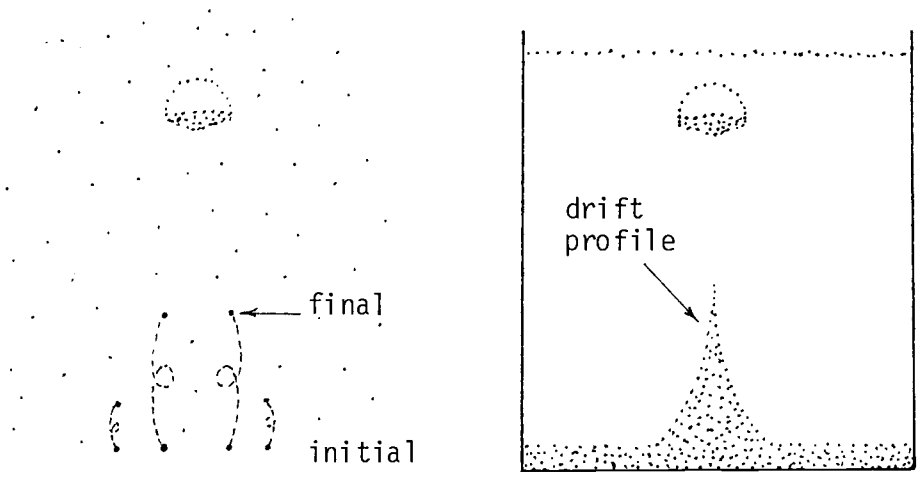

In the large particle regime, Geldart and Cranfield (9) think that the drift induced motion may play a significant role in solids movement which is not predicted by the Kunii-Levenspiel model (2) for vertical solid movement. The model essentially assumes that all of the upward movement is due to solids being conveyed upward in the wake. If drift displacement is disregarded as a major contribution to upward movement, then all of the solids are moving upward in the wake and solids are moving downward in the emulsion phase.

Lateral or radial solids movement are also caused by the passage of a bubble. For lateral movement, Kunii and Levenspiel (2) have postulated a random walk mechanism for solids movement which allows calculation of a lateral solids diffusion coefficient.

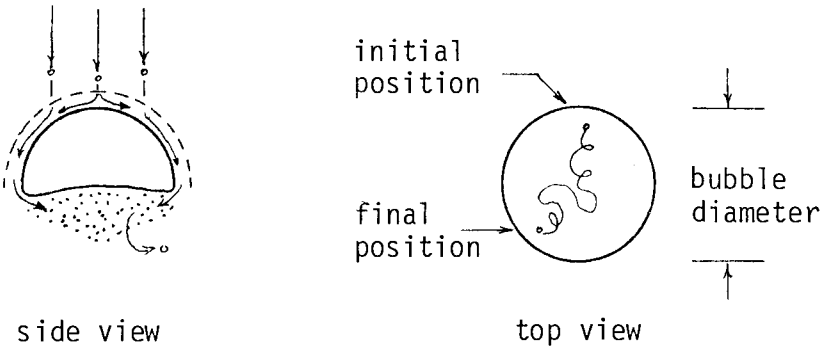

Briefly, the model states that an emulsion particle will enter the well mixed wake of the bubble through the upper half of the bubble from some initial horizontal position and will leave the bubble wake at some final horizontal position. The diffusion coefficient can be derived from the Einstein random walk equation which, in this case, is based on the most probable change in horizontal position of the particle. This model has been used to make successful order of magnitude predictions for $D_{s,\ lateral}$.

MODELS USED FOR CORRELATING SOLIDS MOVEMENT DATA

Models Dealing Only With Internal Bed Behavior

There are essentially two different models which have been used extensively for the correlation of experimental data: the solids diffusion models and the solids turnover rate models. There is also the mechanistic model proposed by Kunii and Levenspiel (2) which has had success in predicting turnover values and radial or lateral diffusion coefficients but hasn't been used extensively as a method of correlating experimental data.

The diffusion models break down into two areas: diffusion models for lateral solids movement and diffusion models for axial or vertical solids movement. The diffusion equation used to describe tracer movement is of the form:

$$\frac{\partial c_t}{\partial t} = D_s \frac{\partial^2 c_t}{\partial x^2}$$

where $D_s = D_{s,\ \text{axial}}$ or $D_{s,\ \text{radial}}$

c_t = tracer concentration

with appropriate boundary conditions

The lateral diffusion mechanism is postulated to be a random walk mechanism caused by solids mixing within the wake behind a rising gas bubble as described by Kunii and Levenspiel (2). The model fits the experimental data within an order of magnitude.

The axial diffusion models assume that tracer particles are mixed by an eddy diffusion mechanism induced by turbulence caused by

a rising gas bubble through the emulsion phase. Poor fits of the experimental data with the model indicate that a diffusion type model cannot satisfactorily explain vertical solids movement. The diffusion coefficients for axial and lateral movement aren't the same; the axial diffusion coefficient being an order of magnitude larger than that of the lateral coefficient. D_s is usually correlated with U_o/U_{mf}.

The solids turnover model for vertical solids movement has been used with experimental tracer data and with direct measurement of solids mass flux values. The vertical solids turnover rate or J_v is simply the total upward or downward mass flux across a horizontal plane in the bed. The tracer technique which has been used in conjunction with the turnover model is based on a very questionable picture of the mechanism of solids movement. The model divides the bed into two well mixed upper and lower regions, each containing total solids of mass W_1 and W_2 respectively. Tracer is present in each region in the concentrations X_1 and X_2 respectively. (mass tracer/mass total solid in region)

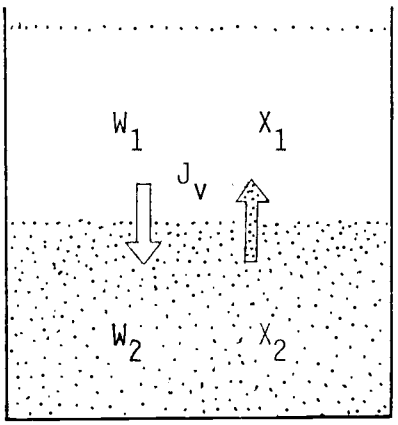

The differential equation describing tracer movement is given as:

$$W_1 \frac{dX_1}{dt} = - W_2 \frac{dX_2}{dt} = J_v A (X_2 - X_1)$$

Where A = the cross sectional area of the bed

and J_v = the solids turnover rate (mass/area-time)

This differential equation is true only in the first few moments of the tracer run. After this time, each region is not well mixed and the tracer at the extreme points from the boundary between the two regions do not contribute any "driving force" for the movement of the solid particles near the boundary. Hence, this tracer technique can provide only an approximate estimate for the upward and downward solids flux or turnover rate in the bed.

Direct measurement of solids mass fluxes should be the more reliable of the two methods for estimating J_v values. There is no reliance upon a questionable mathematical model as in the case of the tracer technique. The difficulty with direct measurement of solid mass fluxes would lie either in the reliability of the calibration procedure or in the transference of a probe calibrated under conditions which may not precisely hold in the bubbling fluidized bed. For example, a probe may be calibrated in a bed at incipient fluidizing conditions which may have a certain solids density or porosity. When the bed is bubbling, the emulsion density may change and the calibration procedure results may become invalid and yield

erroneous results.

Discrete Space and Continuous Time Models

Residence time distribution (RTD) models have been used to model solids RTD's in beds which have constant solids inflow to and outflow from the fluidized bed. The object of this type of modeling is to represent the bed as a combination of discrete, interconnected compartments which are arranged so as to approximate the experimentally obtained solids RTD. The compartments may exhibit well mixed behavior, plug flow behavior or there may be short circuiting around the compartments. Combinations of compartments representing some or all of the above behavior have been used. These models can be referred to as discrete space (compartments) and continuous time (utilize differential equations to represent transient tracer behavior in the network) models. The compartmental arrangement has had no relation to actual regions in the bed which might be represented as well mixed. For example, if there were a reaction occuring between the solids and the fluidizing gas, such a model could be used for prediction of the conversions of exiting solids, but it would be useless for predicting conversions in various regions of the bed. Verloop, et al (3) present a discussion of the various RTD models in use for fluidized beds.

Discrete Space and Discrete Time Models

A compartmental flow model developed by Chang (4) enables one to represent a flow or nonflow (batch) system in terms of well mixed compartments with intercompartmental flows which correspond to actual regions within the real fluidized bed. The model is discrete in space in that it is made up of discrete compartments. The model is also discrete in time in that it makes use of discrete time intervals over which tracer concentration changes occur. By using discrete time notation rather than continuous time notation for the tracer material balance, algebraic rather than differential equations are obtained.

The flow model which enables one to represent actual regions within the bed as well mixed compartments has the utility of being able to predict actual solids conversions within these compartments in the case of reacting solids. In addition, this model can be used to predict exiting RTDs for flow systems. Using the Chang model to represent a coal burning fluidized bed with immersed heat exchange tubes as a series of interconnected well mixed regions would be a useful tool. For example, it would enable a Chemical Engineer to predict where there will be temperature excursions due to poor coal mixing or where the bed might be starved for coal due to the same reason. It is toward this end that the ferrite tracer technique to be described in this thesis is directed. Further details will be presented in the theoretical discussion section.

TECHNIQUES USED IN THE DETERMINATION OF SOLIDS MOVEMENT

Tracer Methods: Types of Tracers

A Tracer is a material which has a property or properties that enables one to identify its presence in a mixture of otherwise indistinguishable particles or molecules. The tracer concentration will be used in conjunction with a tracer material balance which yields a differential equation describing the flow behavior of the tracer. Since it is assumed that the tracer and non tracer flow behavior is identical, the flow behavior of the bulk material or non tracer is inferred from that of the tracer.

In the case of a fluidized bed, the tracer particles should have identical fluidizing properties as the non tracer material. That is, given a tracer and non tracer particle, the tracer particle should on the average move throughout the bed in the same manner or pattern as the bulk bed material. In order for the tracer and non tracer to behave similarly, the following criteria were thought to be necessary: the particle densities should be the same and the particle diameters should be approximately the same.

In previous experimental work, with a wide range of bulk solids particle diameters used, a variety of types of tracers were used. Highly (5) and May (6) used radioactively tagged particles which consisted of a radioactive isotope which was present within the otherwise indistinguishable particle. Razumov (7), Rowe (8), Geldart (9) and this study used particles with magnetic properties. The ferromagnetic properties made it possible for the tracer to be

separated from a bed sample by use of a magnet or else the ferromagnetic properties enabled detection by use of an inductor coil whose inductance was changed due to the proximity of the tracer particles. Mori and Nakamura (10) used colored tracer particles whose concentrations were determined by variations in reflected light intensity from the bed material sample. A porous tracer particle saturated with a soluble salt has been used by Rowe (11). The bed sample tracer concentration was determined by dissolving the salt and back calculating a tracer particle concentration. Electrically conductive particles were used by Hayakawa (12) in conjunction with a probe which measured bed conductivity changes due to changes in the local tracer concentrations.

Depending on the type of model being used to correlate solids motion, there are different types of tracer release techniques. The tracer may be released in the form of a pulse which is used in conjunction with a partial differential equation which uses a diffusion model in two or three dimensions. There may be a horizontal, well mixed layer of tracer laying above or below a non tracer layer in an initially still bed which is then fluidized and allowed to mix for a certain period and stopped. This method has been used in connection with the turnover model and vertical or axial diffusion models. There may be a vertical well mixed layer of tracer which is separated from a non tracer region by a removable partition which then allows the tracer to mix. This method has been used in conjunction with lateral diffusion models.

Tracer Detection or Sampling Techniques

There are essentially three ways to sample or detect tracer concentration within a bed: in-situ detection, in-situ dynamic bed sampling, and static bed sampling. In-situ detection is the direct measurement of tracer concentrations within the bed by using a probe located within the bed of fluidized solids. Examples of this method would be the conductivity probe of Hayakawa (12) and the inductance probe used in this study. In-situ dynamic sampling employs a sample thief in various bed locations. While the bed is fluidized, solids samples are removed from the bed at periodic intervals and analyzed for tracer content. Static bed sampling involves two techniques. Stop or "slump" the bed after a time interval and then "freeze" the bed with a solidifying liquid such as paraffin and slice the bed into sections which are then analyzed for tracer. The other method is to simply slump the bed and remove the tracer, layer by layer, with a suction device and analyze for tracer once again.

The inductance probe would have the advantage of not requiring the bed to be slumped and hence disturb the tracer distribution which existed prior to slumping. Also, there is a direct readout of the tracer concentration near the probe. There is no sample removal and no analysis of samples for tracer concentrations. The major limitation of the inductance probe method is the bulk of the probe itself. Since the probe is so large, it couldn't be used for studies which want to investigate solids movement in a bed free of immersed objects. However, the technique is ideally suited for

studies which are investigating solids movement in fluidized beds with simulated heat exchange tubes.

Direct, In-situ Measurement of Solids Mass Fluxes

This method makes use of no tracer and is best suited for determining solids turnover rates (J_v) rather than axial or radial diffusion coefficients. Direct measurement of mass fluxes utilizes a probe which is immersed in the bubbling bed. Solids sweeping past the probe then cause some change in the probe output signal which has been previously calibrated for known mass flux values. Direct measurement of fluxes appears to have been used less frequently than tracer techniques. Marshek and Gomezplata (13) developed a thermistor anemometer probe which consisted of two thermistors separated by a short distance. The upstream thermistor was used as a heater element and the downstream thermistor was used as a temperature sensing element. As mass flux past the heater would increase, the temperature downstream would decrease and as a result, the sensor thermistor resistance would also change. The probe could be calibrated for known mass flux values. Razumov (14) made use of a piezoelectric probe where moving solids would impinge on a piezoelectric crystal device. Solids impingement on the device would strain the crystal and cause a low voltage signal to be generated which could then be amplified and calibrated. Also within this category would be the strain gage probe technique investigated in this study.

SOLIDS MOVEMENT STUDIES IN THE LARGE PARTICLE REGIME

There have been few other studies of solids mixing in the large particle regime. Brötz (15) appears to have been the first to find axial diffusion coefficients for particle diameters of 2-10 mm (0.08 - 0.33 inch). Colored particles were used as a tracer and the bed was apparently dissected in order to determine tracer concentrations at various bed levels. Burovoi and Svetozarova (16) found axial diffusion coefficients of 0.5 - 4.0 mm (0.02 - 0.16 inch) particles by H_2O evaporation kinetics in a continuous flow fluidized bed. Highly and Merrick (5) have used the largest bed size found in the literature. Coal particles of 0.55 - 1.7 mm (0.022 - 0.067 inch) were used in 1.52 m (5 ft) diameter bed. Radial or lateral diffusion coefficients were found by using a sample thief to remove radioactively tagged tracer particles at various vertical and radial positions in the bed. Geldart and Cranfield (9) studied the vertical movement of 1-2 mm (0.030 - 0.079 inch) particles by using magnetic tracer particles which were removed from non-magnetic material. The turnover or J_v model was used to correlate solid movement. Table 1 summarizes these results.

Table 1 Summary of Large Particle Mixing Studies

Investigator	Bed Dimensions	$\bar{d}_p$	U_o/U_{mf}	Mixing Parameters	Measurement Technique
Brötz(1956)	D=6 cm (2.4 in) H=48 cm (19 in)	2-10 mm	1.3 - 2.3	$D_{s,a}$= 0.9-11.0 cm^2/sec	Two vertical layers of colored tracer particles
Burovoi and Svetozarova (1965)	D=? H=28 cm (11 in)	0.5-4 mm Zn-Cu ore	2.0	$D_{s,a}$= 35-90 cm^2/sec	H_2O evaporation kinetics in a continuous flow bed
Highly (1969)	D=5 ft (152 cm) H=1,2 ft (31,61 cm)	0.55-1.7 mm coal mix	4-7	$D_{s,r}$= 67 cm^2/sec	Radioactive tracer pulse with in-situ sampling
Geldart and Cranfield (1972)	H=15 cm (6 in) 61x2 cm (2 ft x 0.8 in)	1-2 mm alumina	1.17-2.67	J_v = 0.08-1 gm/cm^2-sec	Two vertical layers of solids, one layer is magnetic tracer

II. PRELIMINARY BED INFORMATION AND EXPERIMENTS

BED ARRANGEMENT AND AIR SUPPLY

Figures 1, 2 and 3 show the bed and test section used for testing the prototype devices. The test section was a 24 inch (61 cm) high 12 inch (30.5 cm) wide and 12 inch (30.5 cm) deep unit with two removable plywood panels for the mounting of instruments. The bed distributor plate consisted of 7/32 inch (5.6 mm) holes drilled on 1 inch (2.54 cm) centers, amounting to an open area of 3.8 percent. Sand was loaded into the bed through a conical hopper located on the upper portion of the bed section. The bed was dumped using a valve located at the bottom of the bed just above the distributor plate.

Air was supplied to the bed by a Roots type compressor with a maximum capacity of 8000 cfm at 1 psi. The compressor was driven by a Caterpillar 325 h.p. Diesel engine. Ducting with a one square foot cross sectional area and lined with dampening material brought the air to the bed and helped to attenuate any periodic pressure fluctuations due to the lobe type compressor. Precise measurement of air flowrate supplied to the bed was accomplished by use of a calibrated orfice plate. Careful control of air flowrate was accomplished by using a combination of air bypassing and diesel engine running speed adjustment.

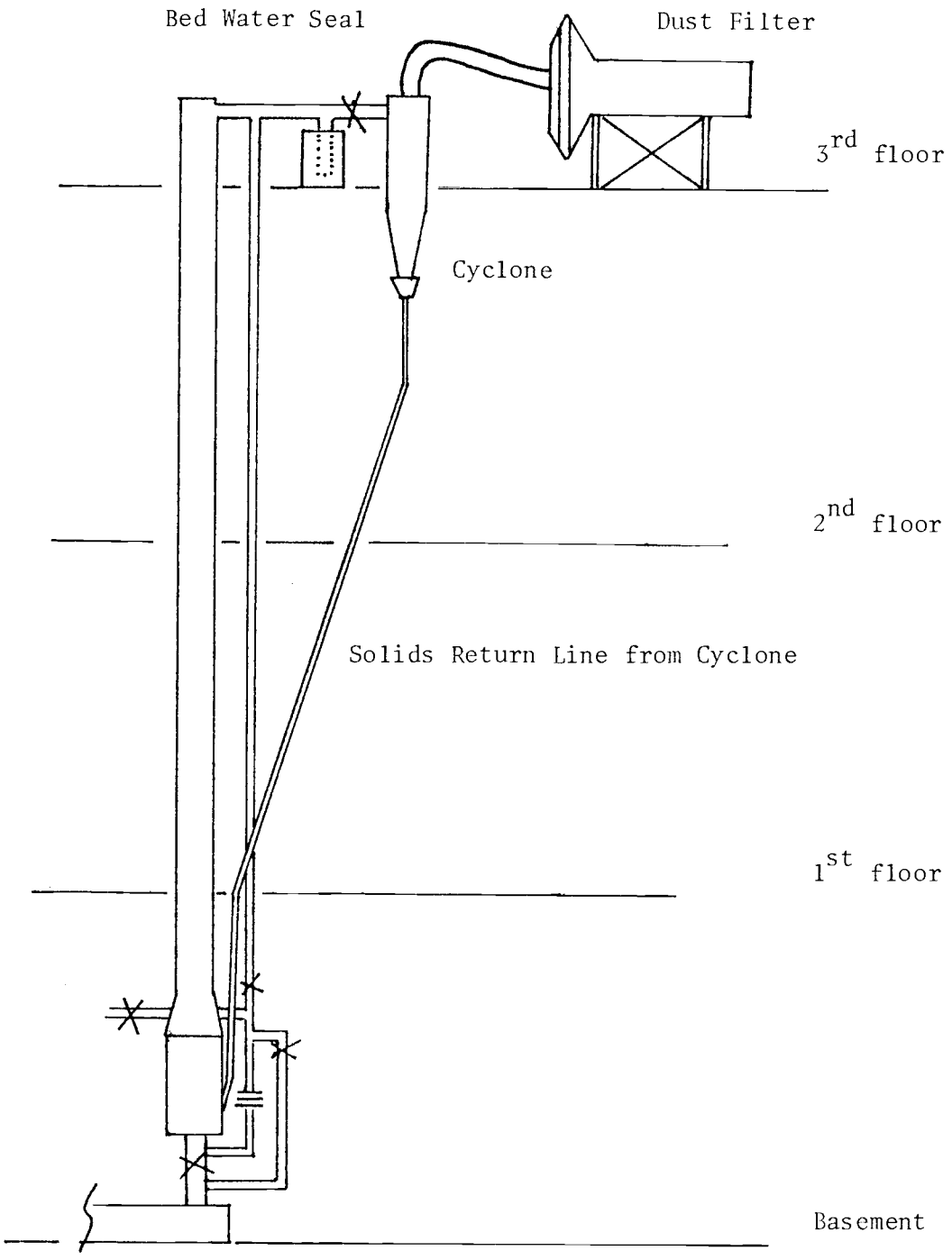

Figure 1 The Overall Small Fluidized Bed System

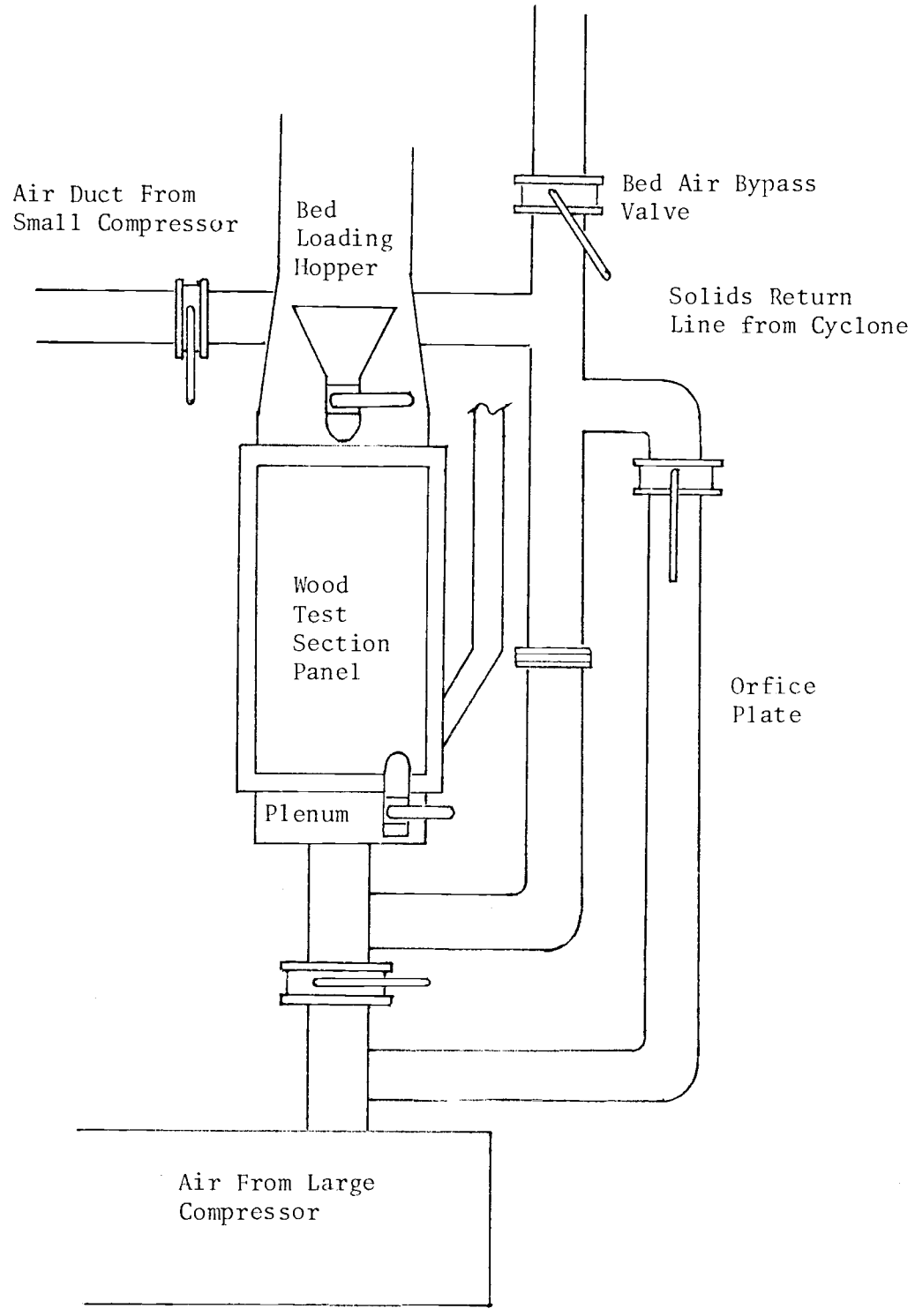

Figure 2 Air Supply Details for the Small Bed

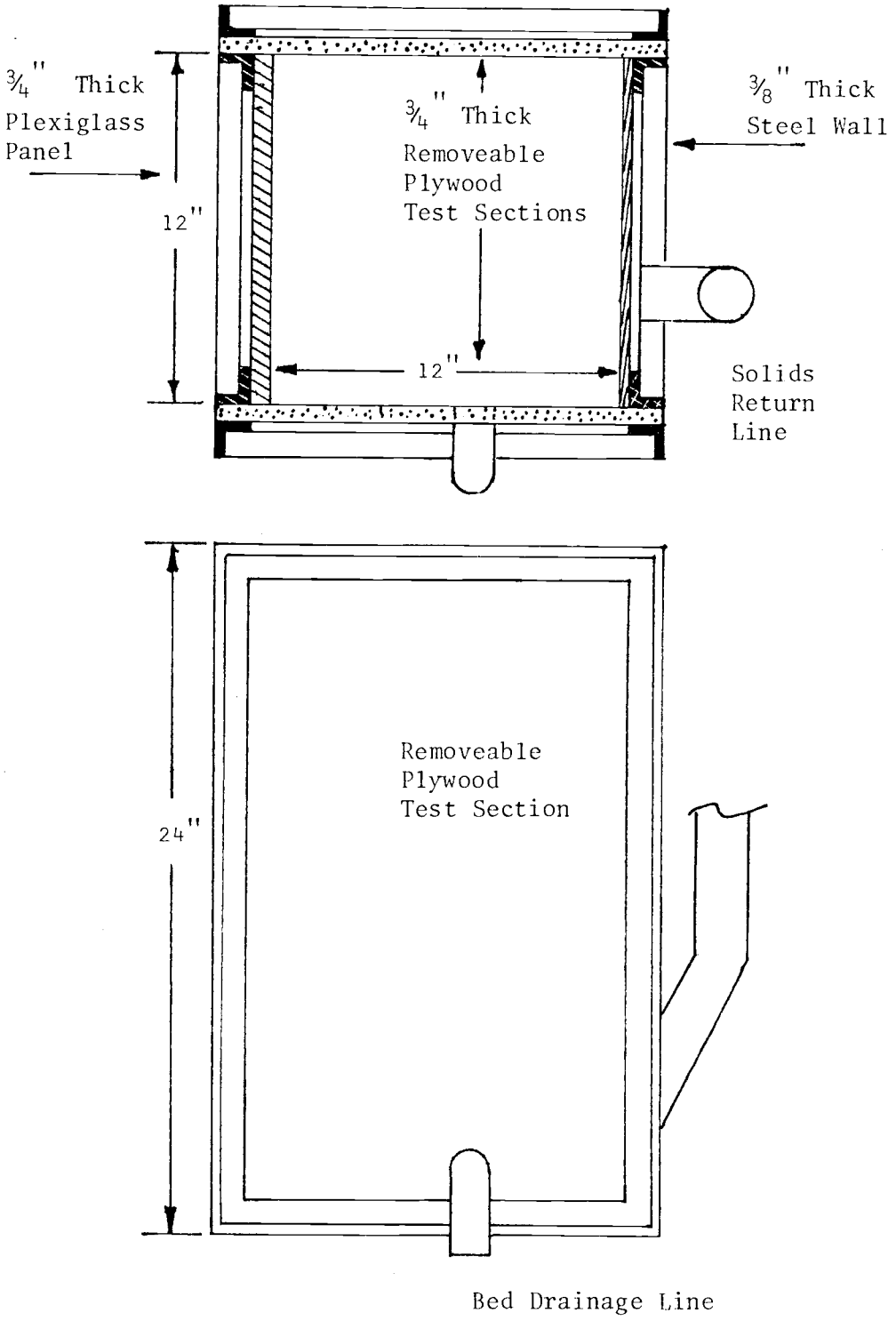

Figure 3 Details of the Small Fluidized Bed Test Section

WEIGHT DISTRIBUTION OF PARTICLE SIZES

Rather than have a single size of particles in the bed, it was decided to have an exponential numbers distribution with the density function of the form:

$$f_n(d_p) = \lambda \cdot \exp(-\lambda\, d_p)$$

It turns out that when the sands available are EI-8, EI-16, and EI-20 silica sand and they are mixed in the volume ratios of 5:3:2 respectively, they will approximately make a number distribution with $\lambda = 4$. Converting this number distribution to a weight distribution, one obtains a density function of the form:

$$f_w(d_p) = 42.7\ \ d_p^3\ \ \exp\ (-4d_p)$$

Using the 5:3:2 volume ratios yields an empirically obtained mean particle diameter of $\bar{d}_p = 0.96$ mm (0.038 inch). Plotted in Figure 4 is the theoretical weight distribution and the actual obtainable weight distribution. Checks of the size distribution after using the sand for the experiments indicated that the mean particle diameter is the same and that there was no apparent attrition of the large sand particles. Some of the fines below $d_p = 0.10$ mm (0.004 inch) had elutriated out of the bed but they had a negligible effect on the size distribution.

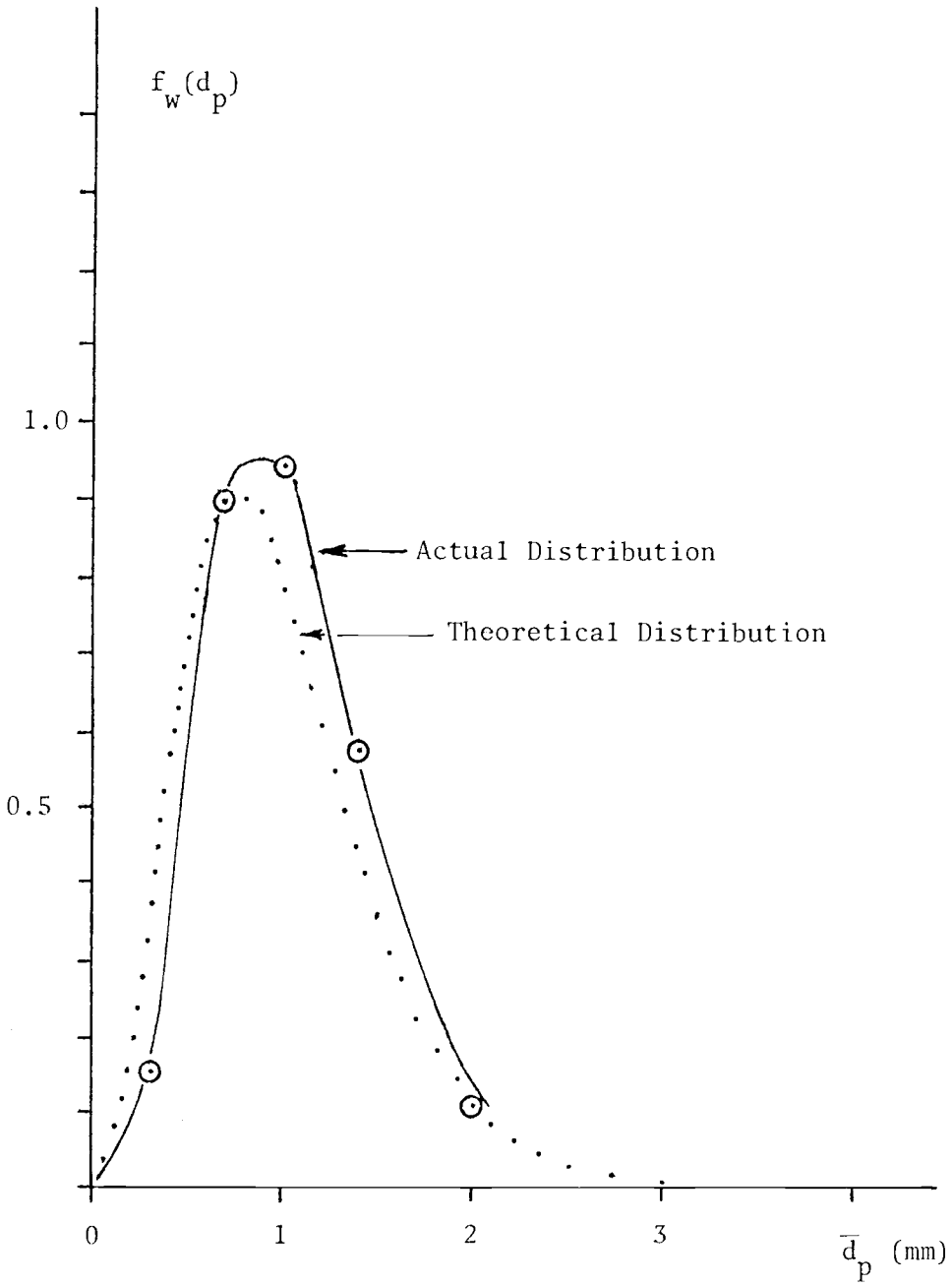

Figure 4 Density Function of Particle Weights

vs.

Particle Diameter

PRELIMINARY EXPERIMENTS

Using the exponential size distribution previously described, the various properties of the bed at minimum fluidizing conditions were determined:

L_m = 11.5 inches (29.2 cm)

L_{mf} = 12.0 inches (30.5 cm)

U_{mf} = 1.1 ft/sec (0.335 m/sec)

ρ_{mf} = 81.8 lb/ft^3 (1.31 gm/cm^3)

ρ_s = 163 lb/ft^3 (2.62 gm/cm^3)

Minimum fluidizing velocity was found by plotting bed pressure drop versus superficial air velocity through the bed. Results of the experiment are plotted in figure 5. Bed pressure drop at U_{mf} was found to be not equal to the static head of the bed, but was lower by about 30 percent. The theoretical static head of the bed at L_{mf} was 18.4 inch water (0.66 psi, 4.58 kPa) while the experimental value was 13.0 inches of water (0.47 psi, 3.24 kPa). This low value for bed pressure drop is attributed to possible short circuiting of air through the bed and was found to be repeatable at minimum fluidizing conditions.

INSTRUMENTATION USED FOR EXPERIMENTS

The tape recording of all experimental runs was accomplished with a Hewlett-Packard 3960 four channel FM Instrumentation recorder.

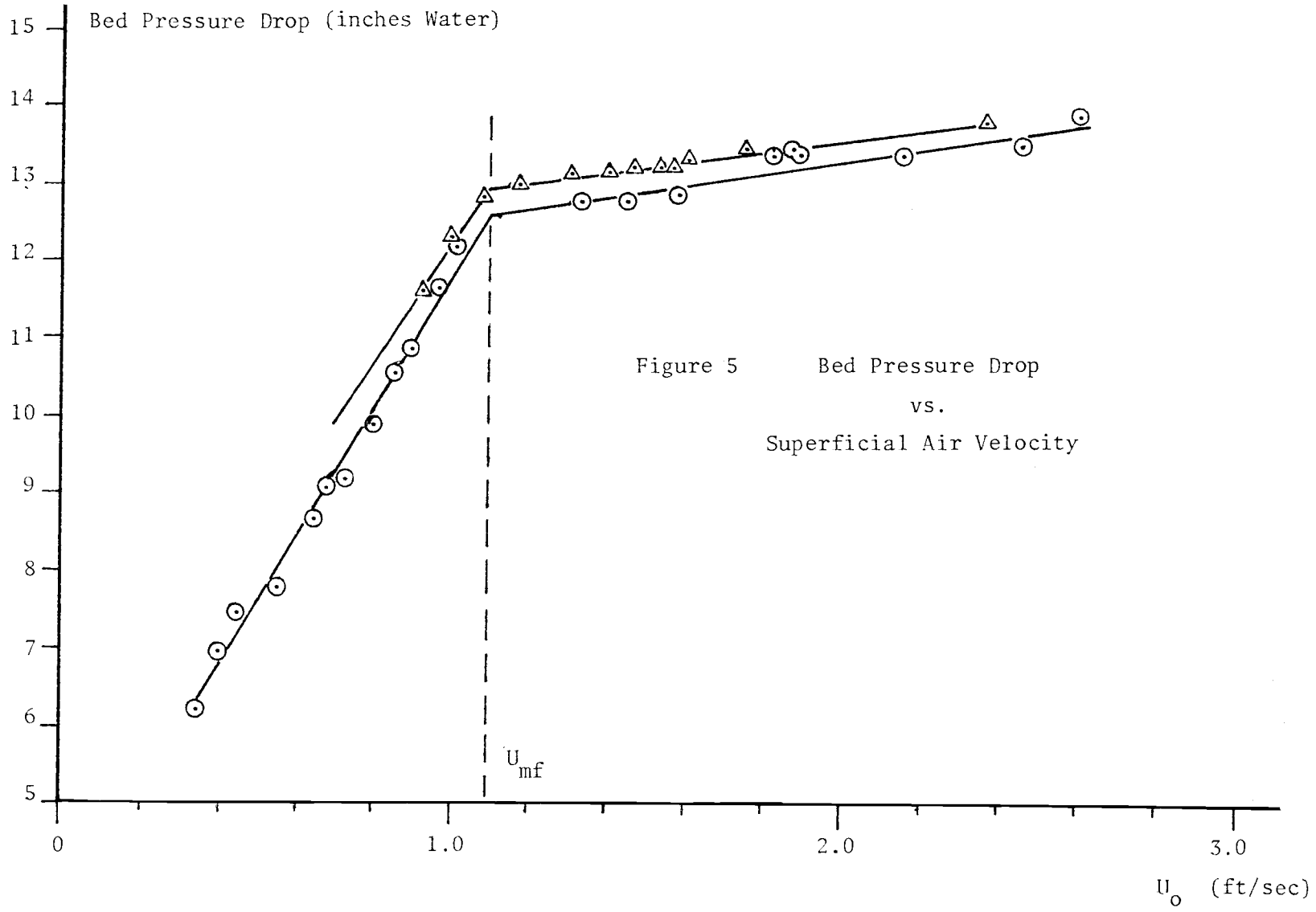

Figure 5 Bed Pressure Drop vs. Superficial Air Velocity

A Hewlett-Packard 7402A,2 channel strip chart recorder was used for continuous monitoring of experimental runs and for the replaying of taped data.

III. THE STRAIN GAGE PROBE METHOD FOR SOLIDS MOVEMENT MEASUREMENT

INTRODUCTORY COMMENTS

The use of a probe which would deflect when immersed in a bed of moving fluidized solids was first suggested by Dr. Octave Levenspiel. The technique involves the use of opposing strain gages mounted on the base of the probe beam which are in an active bridge amplification circuit. When the beam deflected up or down, the circuit output voltage would swing positive or negative respectively. The probe would respond to the mass flux of solids passing the probe. Torque acting on the probe may or may not be a linear function of solids mass flux, but a calibration procedure would still enable one to obtain a relationship between mass flux past the probe and the bridge circuit output. Gibson and Fasching (7) report using a beam with attached strain gages which was used for the flow metering of low density aerated coal dust particles. This is the only reference encountered which resembled the strain gage probe method of this thesis.

The experimental application of the probe in the bed would involve the use of multiple probes which would be used to obtain a continuous record of instantaneous mass flux values past each probe. The instantaneous mass flux values would then be separated into their upward and downward components and each would then be time averaged. The upward mass flux averages from each probe would then be averaged with each other as would the downward values. From these mass flux

values can be calculated a vertical solids turnover rate. These turnover rates would then be compared with those obtained from the inductance probe results.

THEORETICAL CONSIDERATIONS

The Torque Motor Calibration Technique

If the probe and its accompanying circuitry could be immersed in a bed of solids which were moving at a known mass flux rate, the calibration procedure would be a simple one step method. Since it isn't possible to easily obtain a known mass flux and use a "live" probe simultaneously, a two step method was devised for the calibration of the strain gage probe. First, find the relation between solids mass flux past a dead or dummy probe immersed in the bed and the resultant torque acting on the probe. Then, with the live probe outside the bed, dead weight load the probe and record the accompanying bridge circuit output.

Step one was accomplished in the following manner as illustrated in figures 6 and 7. The dummy probe was rotated through a bed of solids at minimum fluidizing conditions in order to eliminate the contacting of bubble voids by the probe. A constant rate of rotation, n (rev./min.), is maintained by a servo controlled motor with torque indicating output. Hence, with this method, a series data points of torque (τ) versus average solids velocity ($\overline{V}_s$) sweeping past the probe can be obtained.

The following equation is used for relating solids mass flux, (mass/area-time), to average solids velocity:

$$(1) \qquad \underline{\underline{\Phi}} = \overline{V}_s \cdot f_s \cdot \rho_{mf}$$

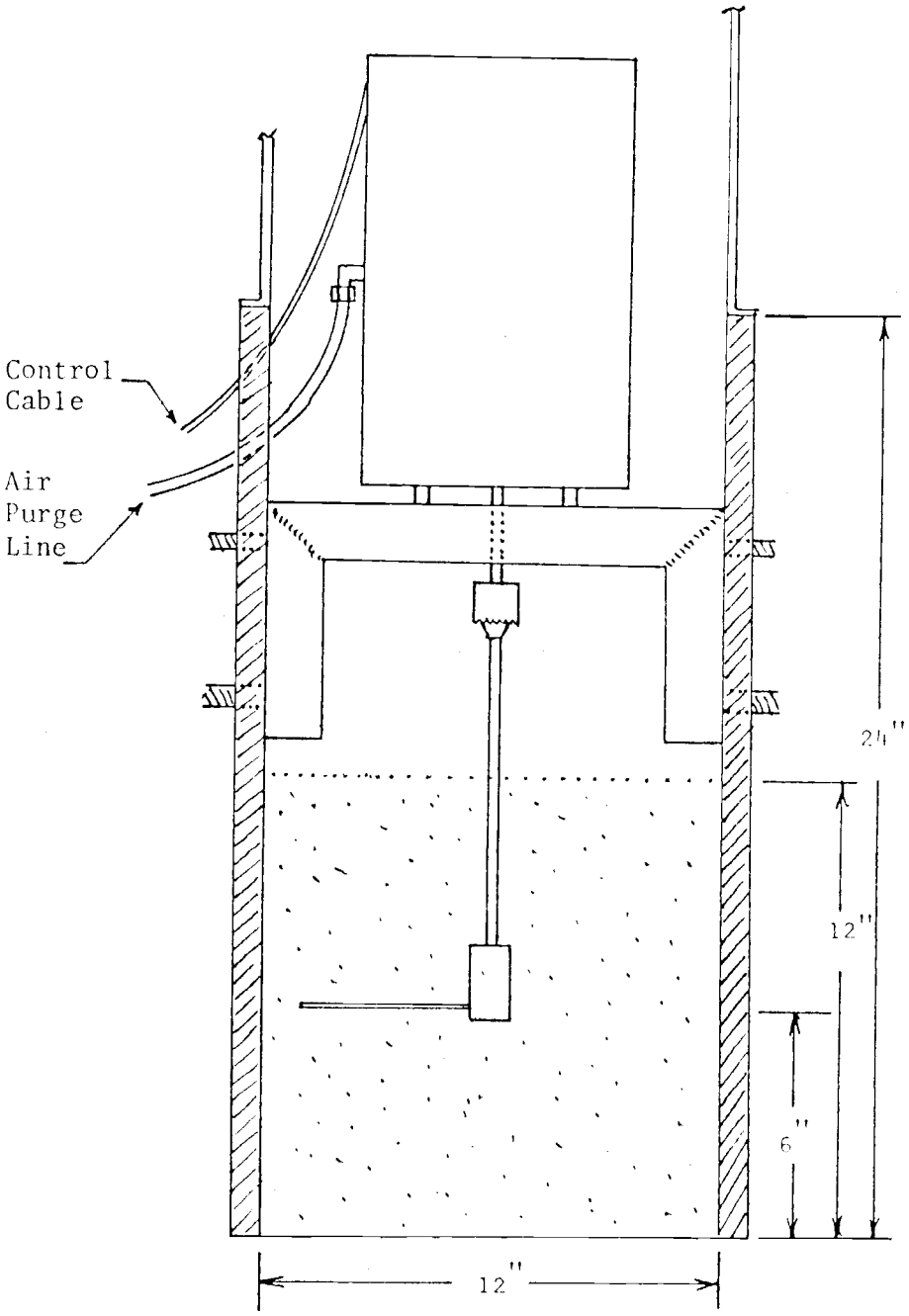

Figure 6 Torque Motor Placement in the Bed

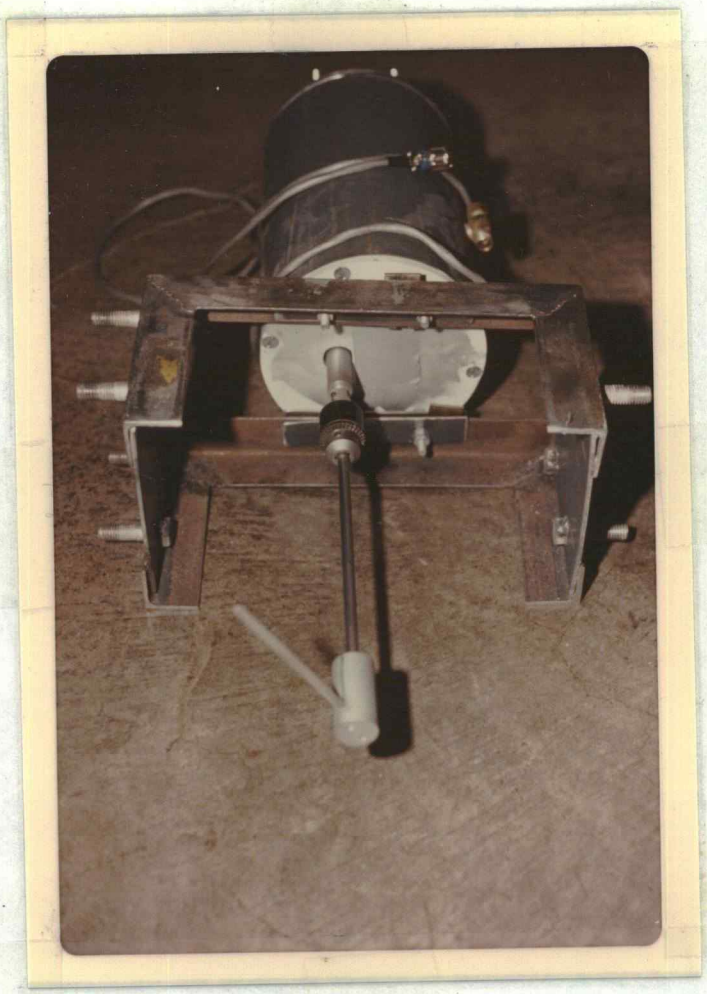

Figure 7 Photograph of the Torque Motor Unit

where f_s = the fraction of the probe length which is contacted by solids at ρ_{mf}

ρ_{mf} = the density of the solids emulsion phase at minimum fluidizing conditions.

Since the velocity of the solids sweeping past the probe is a linear function of the probe length, the mean solids velocity sweeping past the probe is:

$$(2) \quad \bar{V}_s = \bar{R} \cdot n \cdot 2\pi$$

where R = the centroid of the dummy probe

n = the frequency of rotation of the probe

Based on equation (1) the following hypothetical curve can be obtained for $\bar{\Phi}$ versus f_s:

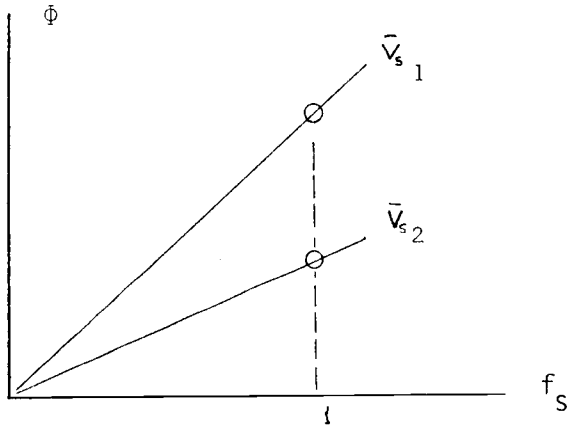

Now, using the data at U_{mf} obtained from the above figure, and the accompanying τ values, a calibration curve can be obtained as in the hypothetical figure below.

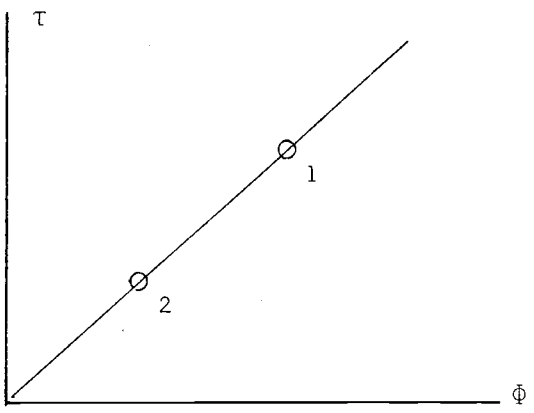

The τ versus $\bar{\Phi}$ curve is now known and should be valid for the actual live strain gage probe, assuming that the emulsion phase solids density for the bubbling bed is the same as ρ_{mf}.

Strain Gage Probe Theoretical Considerations

The strain gage is a resistor which is sensitive to stretching or to an applied stress which results in strain of the gage substrate material. The strain (length of elongation/unit length) will cause a change of ε in the unstrained gage resistance R. The gage consists of a grid of conductive material on a flexible mounting material. When a strain is applied along the axis of the grid, the resistance changes by + or - ε depending on whether the strain is one of tension or compression respectively.

Since there will be an exciting voltage used for the gage resistance grid, there will be heat dissipation from the grid due to resistance heating. Because of this resistance heating effect, the gage must or should be bonded to a good heat sink material such as a

metal or there should be good convective cooling of the top of the gage.

The gage is used in conjunction with a bridge type detection circuit in which the gage is one of the arms of the resistance bridge. For the purposes of this study, four gages were used in the probe circuit. Two of the gages were located 180° apart from each other on the probe rod. By mounting the two active gages in such a manner, the upper gage would be under tension with resistance change of $+\varepsilon$ while the lower gage would be under compression with resistance change of $-\varepsilon$. This method doubles the probe sensitivity and enables one to discern whether the probe is deflecting vertically up or down. The remaining two gages were mounted on the base unit of the probe and are denoted as passive gages. The two passive gages were used as temperature compensating resistors which were intended to compensate for ambient temperature induced resistance drift of the two active gages. Figure 8 shows the bridge circuit used for the four strain gages. The basic bridge circuit is analyzed as follows:

R_{11} and R_{22} are temperature compensating gages
R_1 and R_2 are active gages where R_1 can be represented as $R+\varepsilon_1$ and R_2 can be represented as $R+\varepsilon_2$

For this type of bridge circuit,

$$(3) \qquad \frac{V_{out}}{V_{excite}} = \frac{R_{11} R_1 - R_{22} R_2}{R_{11} R_1 + R_1 R_2}$$

Without Balancing Adjustment

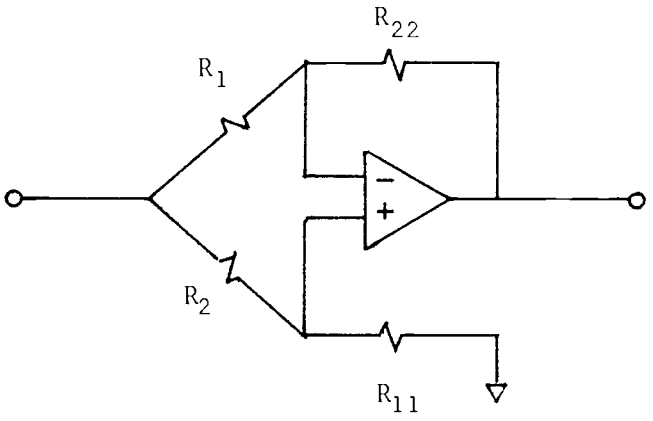

With Balancing Adjustment

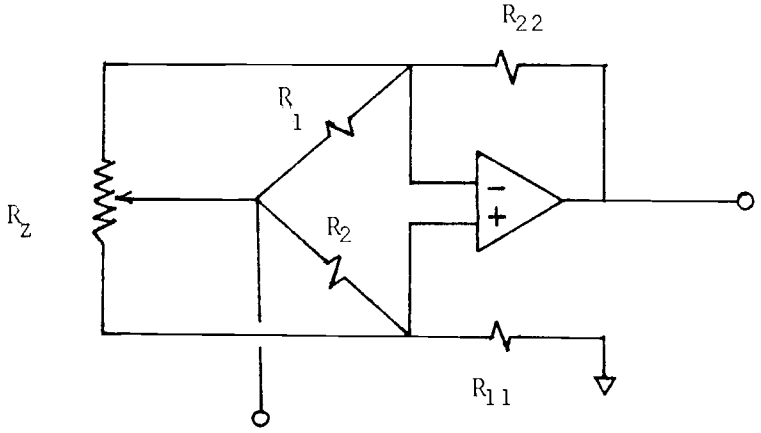

Figure 8 Bridge Amplifier Circuits

substituting for R_1 and R_2 yields upon manipulation:

$$\frac{V_{out}}{V_{excite}} = \frac{R(\varepsilon_1 - \varepsilon_2)}{2R^2 + R(\underbrace{2\varepsilon_1 + \varepsilon_2) + (\varepsilon_1\ \varepsilon_2}_{\text{Negligible terms.}})}$$

Hence,

$$(4) \quad \frac{V_{out}}{V_{excite}} = \frac{\varepsilon_1 - \varepsilon_2}{2R}$$

When the top gage (R_1) is in compression (upward flow) ,

$$R_1 = R-\varepsilon \quad \text{(top gage)}$$

$$R_2 = R+\varepsilon \quad \text{(bottom gage)}$$

Hence, $\varepsilon_1 = -\varepsilon$

$\varepsilon_2 = +\varepsilon$

And: $$\frac{V_{out}}{V_{excite}} = \frac{-\varepsilon}{R}$$

Conversely, when the top gage is in tension downward flow):

$$\frac{V_{out}}{V_{excite}} + \frac{\varepsilon}{R}$$

The small signal V_{out} must then be amplified up to recordable levels and is done so with the complete amplifier circuit as shown in figure 9. The variable resistor R_z is used for initially zeroing or balancing the bridge because of residual strain in the gages due to mounting. A gain of 1000 is used to bring the bridge amplifier output up to recordable levels.

Signal Processing After Amplification and Recording

The expected output from the strain gage probe in a bubbling fluidized bed was thought to be similar to that illustrated in the figure below.

In this figure, there will be short, high mass fluxes moving upward which would be caused by rapid passage of the wake behind a bubble. There would also be longer, lower mass fluxes moving downward caused by solids dropping or slipping downward. The sharp upward peaks would be of the same frequency as bubbles passing upward through the bed.

In order to find an average upward mass flux and an average downward mass flux, the output signal from the strain gage probe

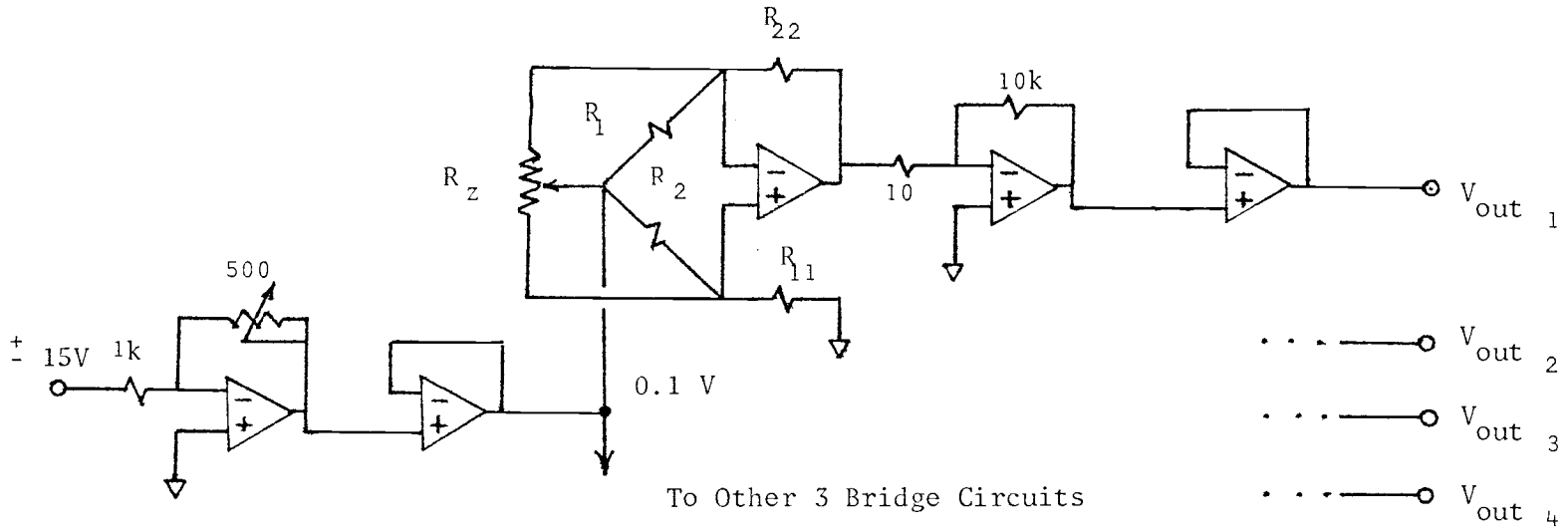

Figure 9 Strain Gage Probe Bridge Circuit

amplifier must be split into a positive and a negative voltage signal corresponding to the upward and downward mass fluxes respectively. The split or rectified signals must then be averaged over a sufficiently long period so that the averaged signals will be smooth ones. The circuit used is shown in figure 10. Amplifiers 1 through 3 are part of an analog subtractor section which will subtract any offset signal that is present in the recorded probe output signal $V_{recorder}$. Amplifier 4 is a precision rectifier section. Amplifier 5 is the moving average filter used to smooth the rectified signal. The averaged signals then go to a strip chart recorder for visual inspection.

The output signal from the probe amplifier section was attenuated by 1/2 so that it would not over drive the tape recorder. Since the tape recorder output is 1/2 of the original input signal to the recorder, during the filtering of the rectified signal, it is doubled in order to correct for the attenuated signal. The data logging and playback scheme is shown in figure 12.

Calculating Turnover Rates From The Rectified and Averaged Signals

Once time averaged voltage signals are known for upward and downward solids motion, the mass flux is found by referring to the calibration curve relating strain gage probe output to mass flux sweeping past the probe. It is assumed that each probe measures the flux passing through one fourth of the bed cross sectional area. Hence, the turnover rate is found as follows:

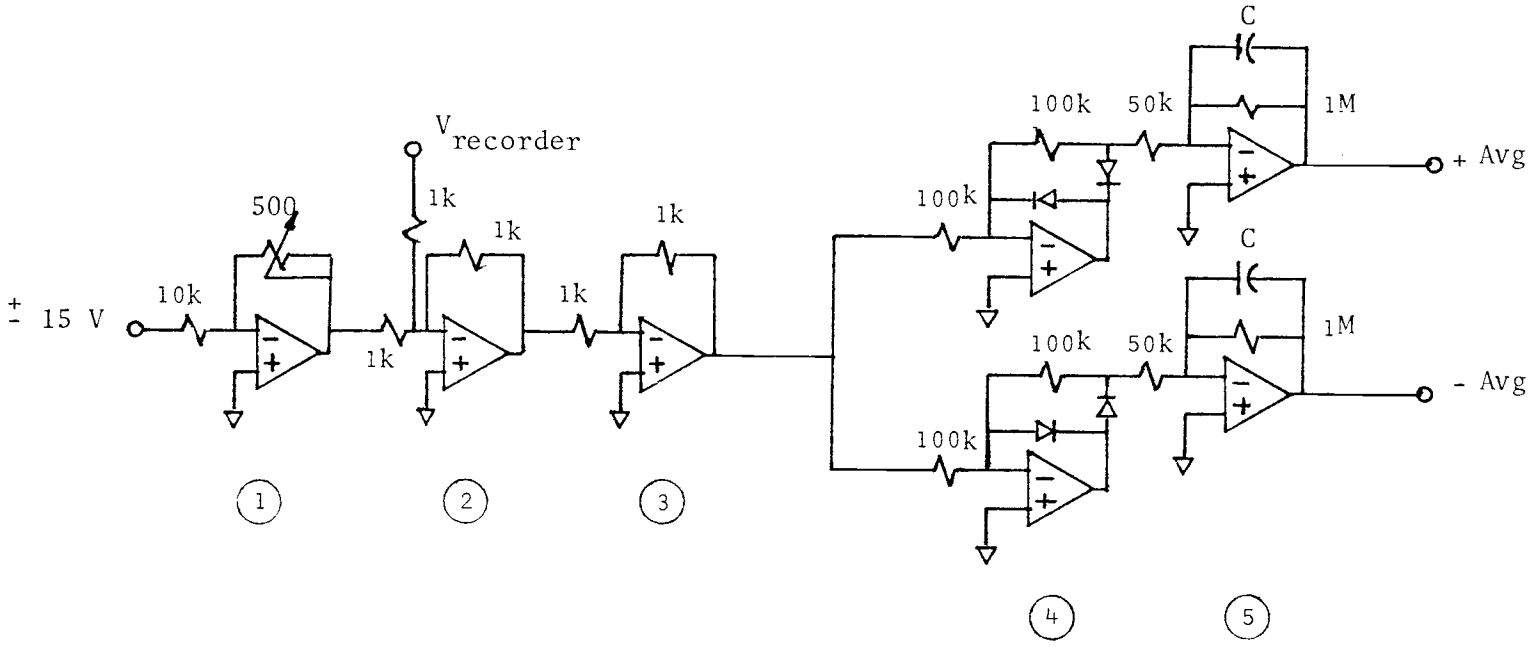

Figure 10 Strain Gage Probe Output Signal Rectifying and Averaging Circuit

C is in μF, R is 1M.
Hence, RC, the averaging period,
is in seconds.

Diodes used are 1N914

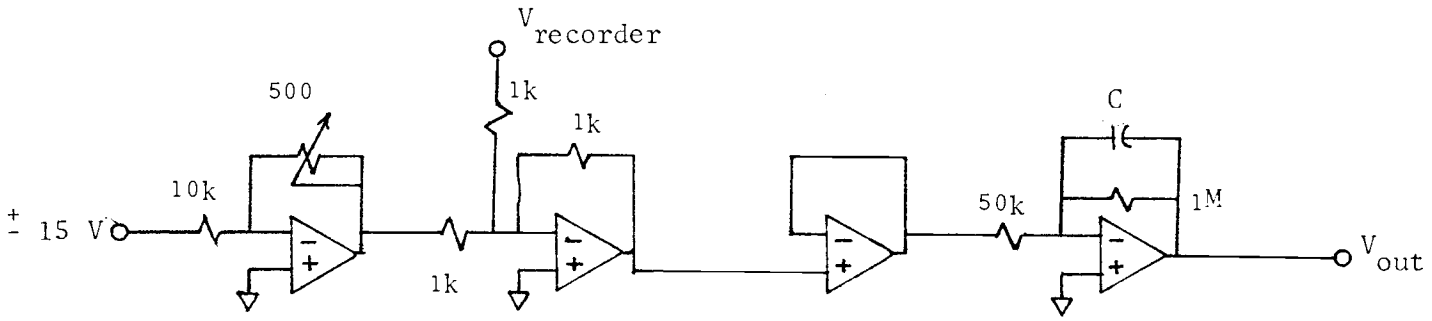

Figure 11 Strain Gage Probe Output Signal Averaging Circuit

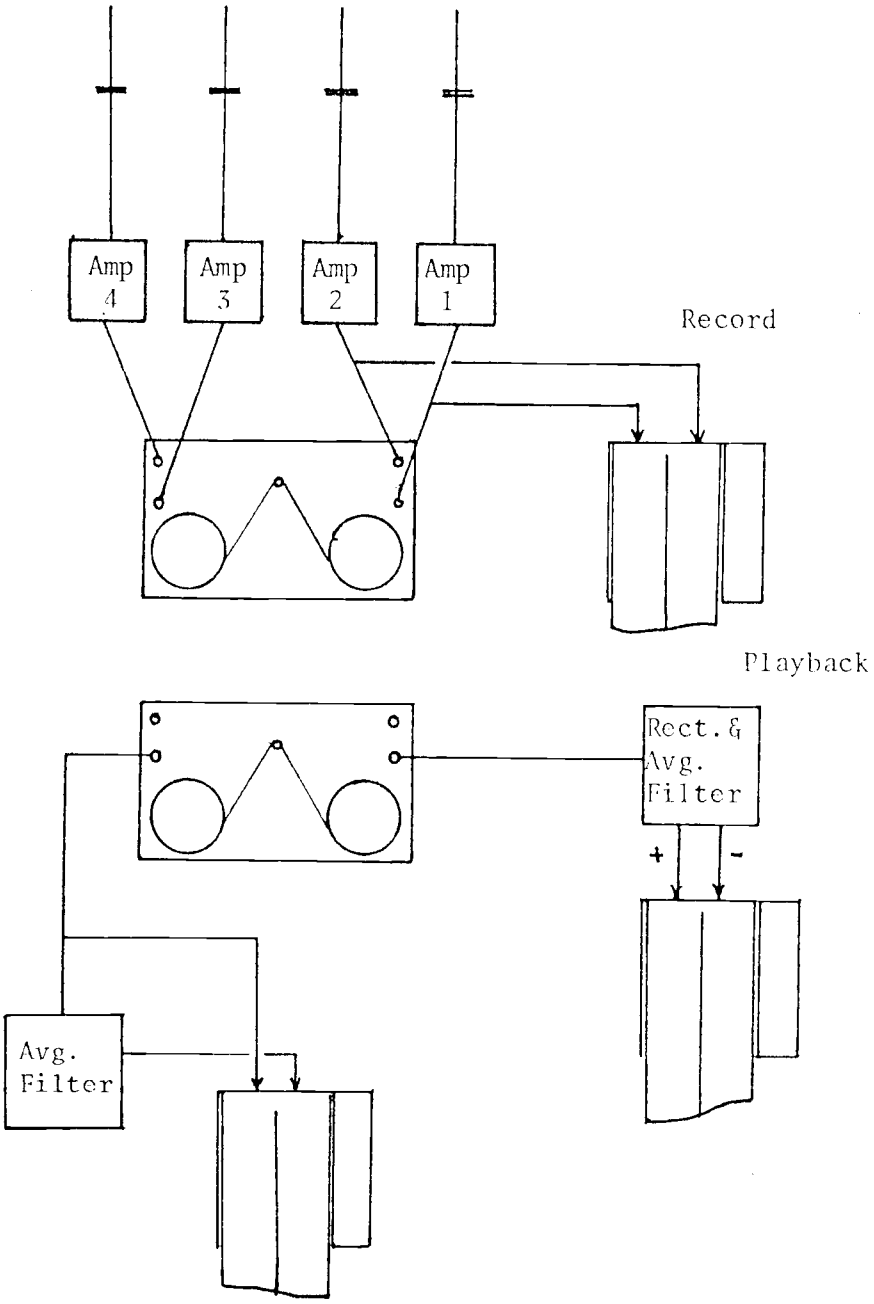

Figure 12 Strain Gage Probe Output Recording and Playback

$$(5)\quad J_v = \frac{1}{4}\sum_{j=1}^{4}\left(\bar{\Phi}_j\right)_{\text{upward}}$$

$$(6)\quad J_v = \frac{1}{4}\sum_{j=1}^{4}\left(\bar{\Phi}_j\right)_{\text{downward}}$$

where $\bar{\Phi}_j$ is the time average upward or downward mass flux moving past probe j

These turnover values can then be compared with the turnover values obtained by the ferrite tracer probe data.

TORQUE MOTOR EXPERIMENTAL WORK AND STRAIN GAGE PROBE CALIBRATION

Torque Motor Experimental Results and Comments

The torque motor used was a Master Servodyne unit manufactured by Cole-Parmer. Torque indicating output from the control unit was logged on a Hewlett-Packard instrumentation tape recorder. The data logging scheme is shown in figure 13. The motor was mounted inside of a 7 inch (17.8 cm) diameter PVC pipe and sealed at both ends. An air purge line was run to the motor casing and was used to keep a continuous flow of air moving past the motor shaft which prevented bed sand from entering the motor casing and damaging the motor. The casing was then mounted on a metal frame which held the unit above the bed surface as is shown in figure 7. The actual dummy probe was located in the middle of the bed of solids at the approximate level where the actual strain gage probes would be located. Details are in figure 14.

Experimental procedure was straightforward. The bed was mixed at 3 U_{mf} for 30 seconds and was then immediately brought down to U_{mf} by opening the air bypass valve to a predetermined position. The run was then allowed to procede until the torque motor output reached a steady value. At this point, the probe RPM was changed and the bed was once again mixed. Throughout the entire experiment the tape recorder was kept running.

It was found that air distribution through the bed at minimum fluidizing velocity was not uniform. As a result, there was a section of slightly denser solids where there was less air moving

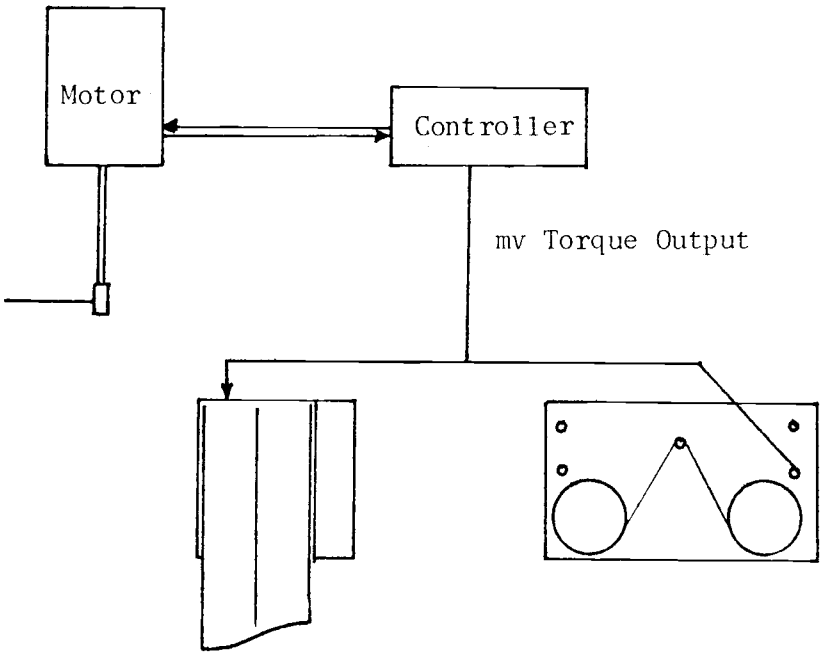

Figure 13 Torque Motor Output Recording Arrangement

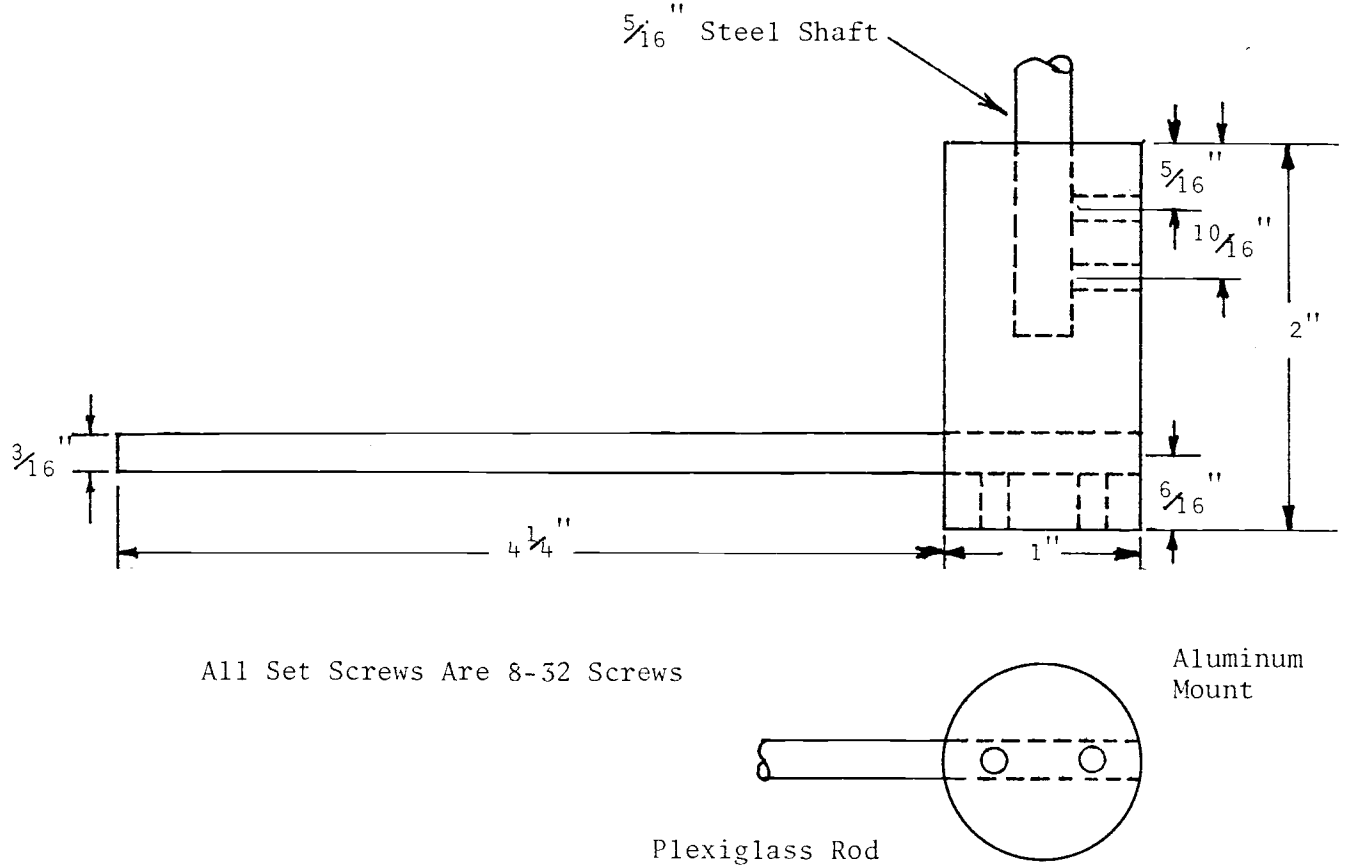

Figure 14 Dummy Strain Gage Probe Details

through the bed. This caused the probe torque output to be periodic with time. Higher torque values were obtained when moving through the dense regions and lower torque values when moving through the less dense regions.

When the bed superficial air velocity was brought down to U_{mf} there would be a decrease in the periodic torque versus time curve until it finally leveled out after approximately one minute. Figure 15 illustrates both the periodicity and drift of the torque curves.

The values of torque which were used for the torque versus RPM calibration curve were the low torque values after the periodic torque values reached a steady state. At first it was thought that the torque value which should be used was the low value immediately after the bed had been "fluffed". These values are plotted in figure 16. The torque versus RPM values do not pass through the origin. In addition, attempts to find torque values below 5 RPM were unsuccessful using this method. The values had poor repeatability and because of this, it was decided to use the low torque values after there was a leveling off of the periodic torque curve. Later use of the strain gage probe indicated a mean torque which corresponded to the torque found in the region below 5 RPM, so only the low leveled off torque values could be used even though they may not be representative of the solids in a fluffed or bubbling bed.

It is thought that the downward drift of torque values may be due to segregation of coarse and fine sand particles in the region swept out by the dummy probe. The coarse sand particles would drop away from the probe leaving behind finer sand particles. Hence, the

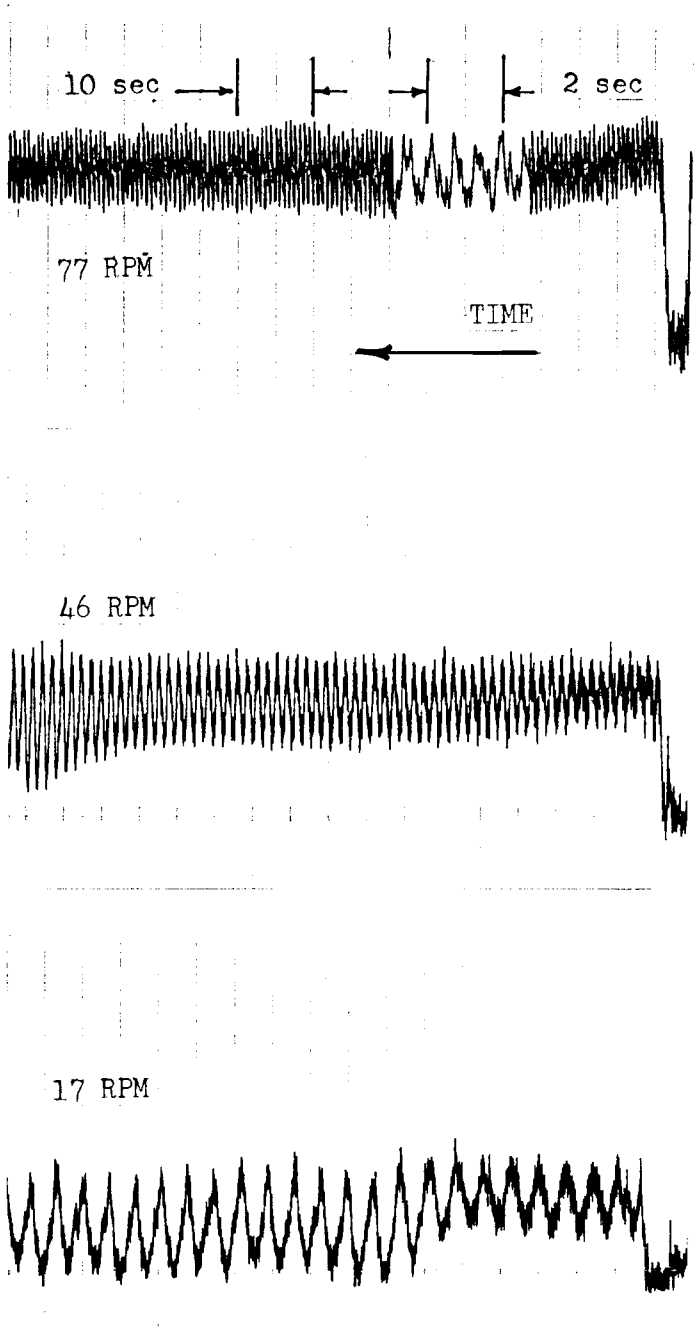

Figure 15 Torque Motor Output Showing Periodicity and Drift

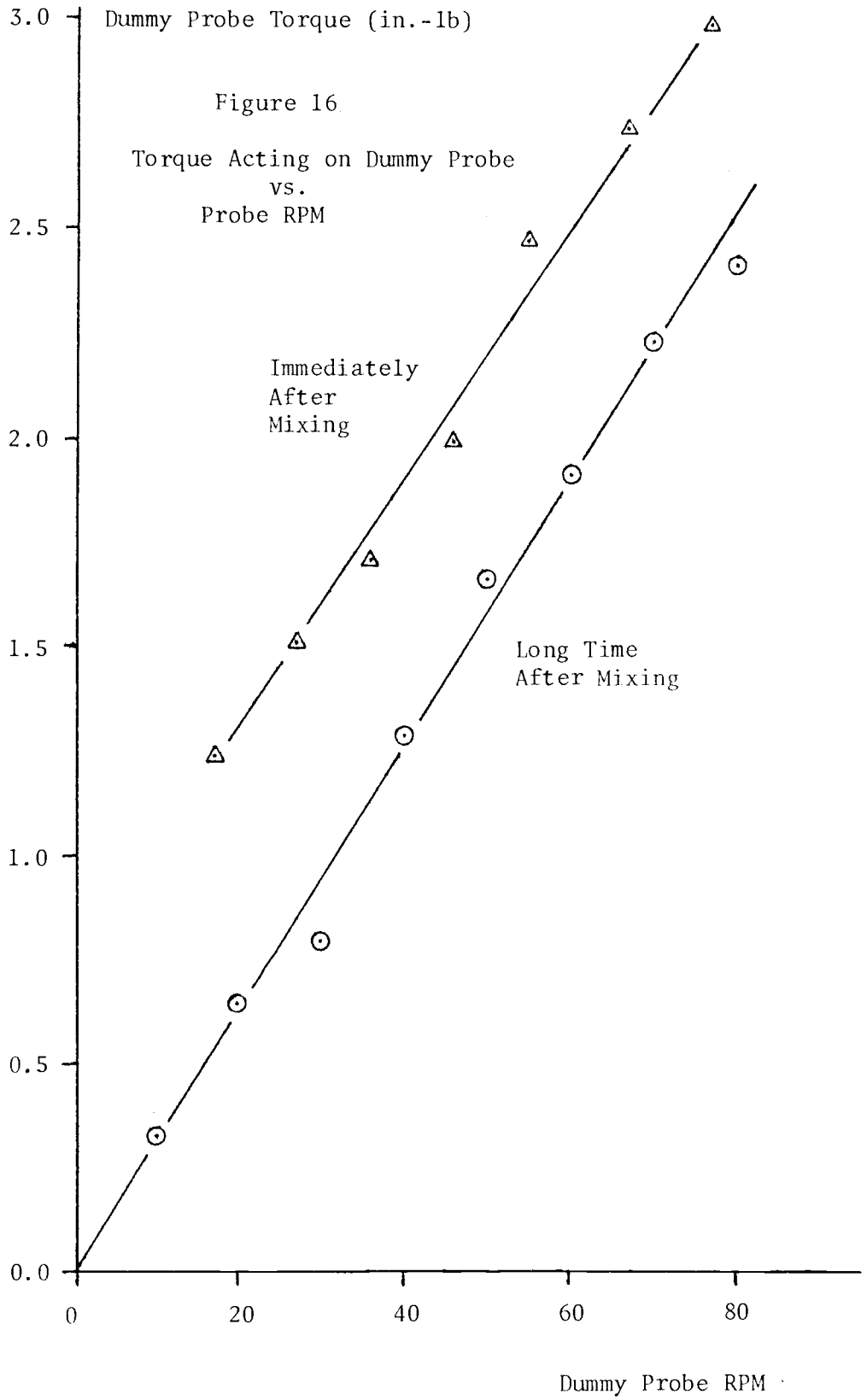

Figure 16

Torque Acting on Dummy Probe
vs.
Probe RPM

torque acting on the probe would decrease. Results of the good experiment for finding probe torque versus probe RPM are plotted in figure 16 and are the data points used to generate figure 17 for probe torque versus mass flux sweeping past the probe. As a check, the dummy probe was removed for a set of runs in order to determine whether there was a torque contribution from the dummy probe mount. It was found that there was no measureable torque contribution from the mount.

Calculating Torque Versus Mass Flux

Given the results of the previous section for τ (torque) and n, (probe RPM), mass flux is found as follows:

$$\bar{\Phi} = \rho_{mf} \cdot \bar{V}_s$$

$$\bar{V}_s = \bar{R} \cdot n \cdot 2\pi$$

$$\bar{R} = \frac{4.25" + 0.5"}{2} = 2.38 \text{ inch } (6.05 \text{ cm}) \quad \text{(from figure 14)}$$

$$\bar{V}_s = (2.38/12 \text{ ft})\ (\text{RPM}/60) \cdot 2\pi$$

$$= (0.02077) \cdot n \text{ ft/sec } (0.6337 \cdot n \text{ cm/sec})$$

$$\rho_{mf} = 81.79 \text{ lb/ft}^3 \ (1.31 \text{ gm/cm}^3)$$

$$\bar{\Phi} = (81.79)(0.02077)(n)$$

$$\bar{\Phi} = 1.6988 \cdot n \quad \text{lb/ft}^2\text{-sec.} (0.8302 \cdot n \ \text{gm/cm}^2\text{-sec})$$

For example, τ = 1.30 in-lb, n = 36 RPM

$$\bar{\Phi} = (1.6988)(36) = 61.16 \text{ lb/ft}^2\text{-sec} \ (29.8 \text{ gm/cm}^2\text{-sec})$$

Results of these calculations are plotted in figure 17.

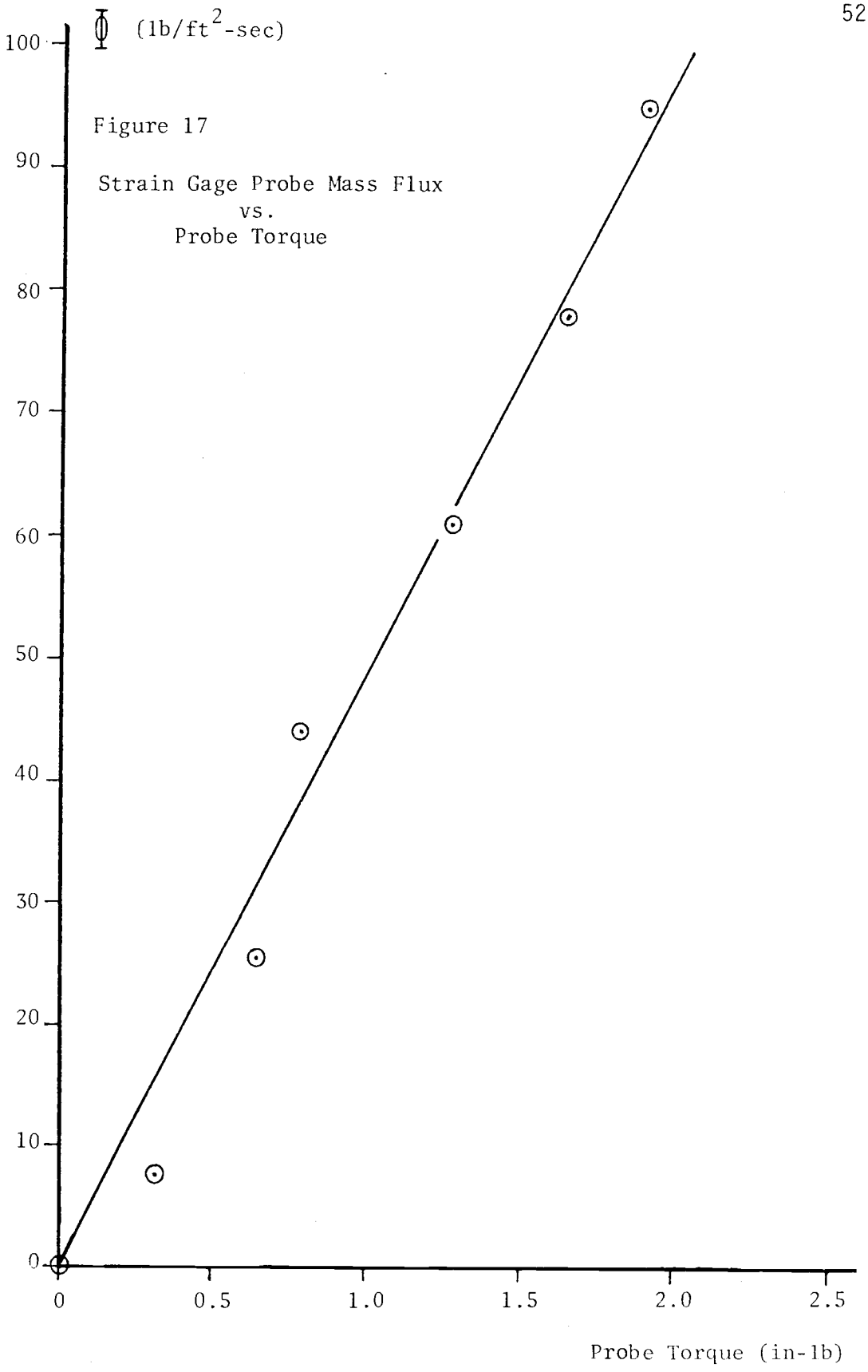

Figure 17

Strain Gage Probe Mass Flux
vs.
Probe Torque

Dead Weight Loading Of The Live Probe

The actual live strain gage probe was loaded with gram weights at a point 4 inches (10.1 cm) from the base of the probe. The torque acting on the probe is:

$$\tau = (4 \text{ in}) (m \text{ grams})$$

The loading was done twice for each probe. The probe was loaded once so that the probe output was a positive voltage then the probe was rotated 180° and loaded so that the probe output was negative. This was done in order to be sure that the same torque would generate the same probe output regardless of the direction of the drag force acting on the probe in the bed. Typical results of the loading procedure are shown in figure 18 for one such probe before silicone rubber shielding was applied. After the gage shielding was done, the loading procedure was repeated and the output was found to be unchanged. An average slope was taken for the probe output versus torque load from the 4 probes and was found to be: 0.2957 in-lb/volt (341 gm-cm volt). The final calibration curve relating strain gage probe output voltage to the mass flux sweeping past the probe is shown in figure 19. This curve was found by using the slope of the curve in figure 17 and the torque/voltage relationship found above.

Hence;
$$\frac{d\bar{\Phi}}{dv} = \frac{d\bar{\Phi}}{d\tau} \cdot \frac{d\tau}{dv}$$

$$= \left(\frac{48 \text{ lb/ft}^2\text{-sec}}{\text{in-lb}}\right) \left(0.2057 \frac{\text{in-lb}}{\text{volt}}\right)$$

$$= 14.19 \frac{\text{lb/ft}^2\text{-sec}}{\text{volt}} \left(6.194 \frac{\text{gm/cm}^2\text{-sec}}{\text{volt}}\right)$$

Figure 18

Strain Gage Probe Output
-vs-
Static Torque Load

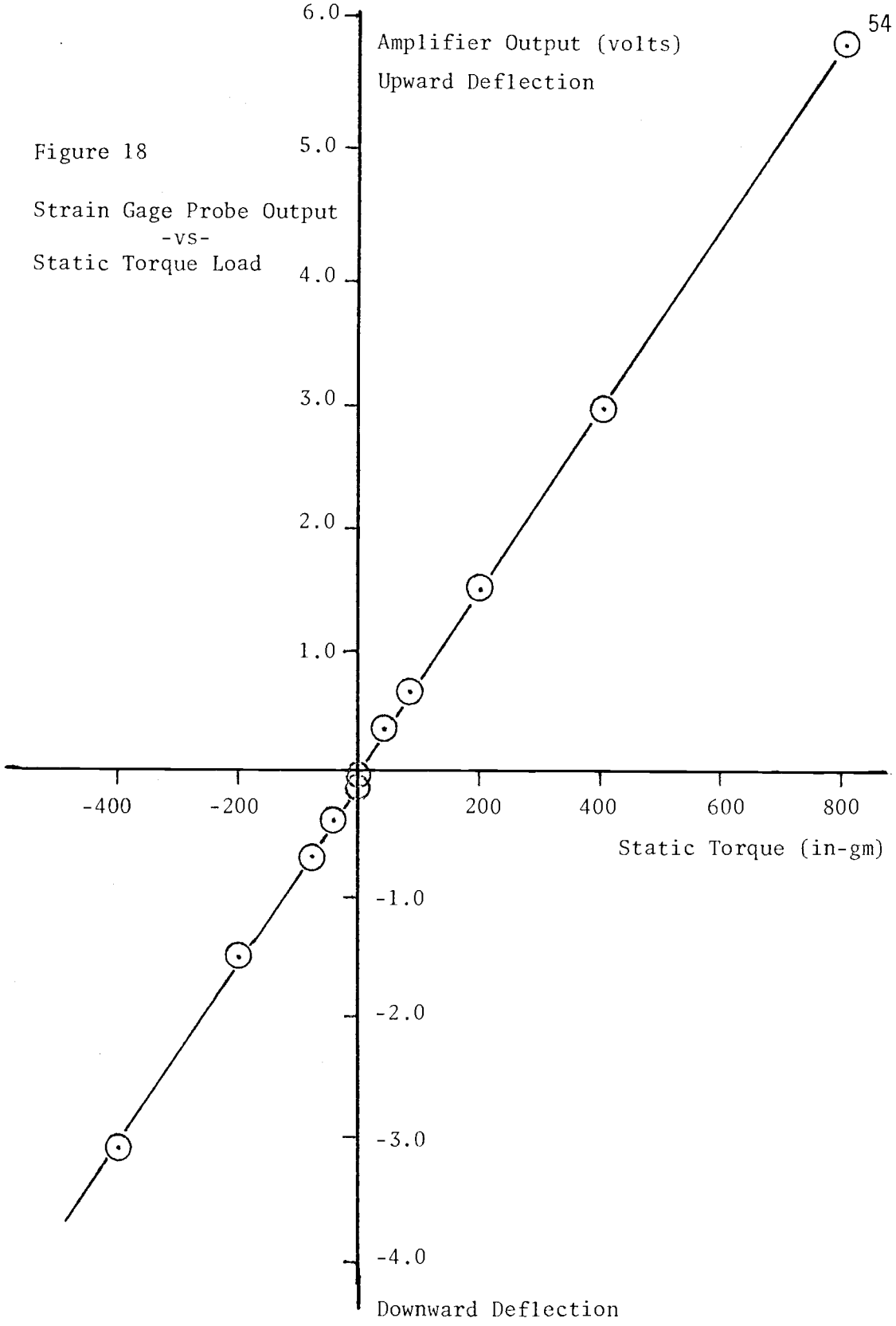

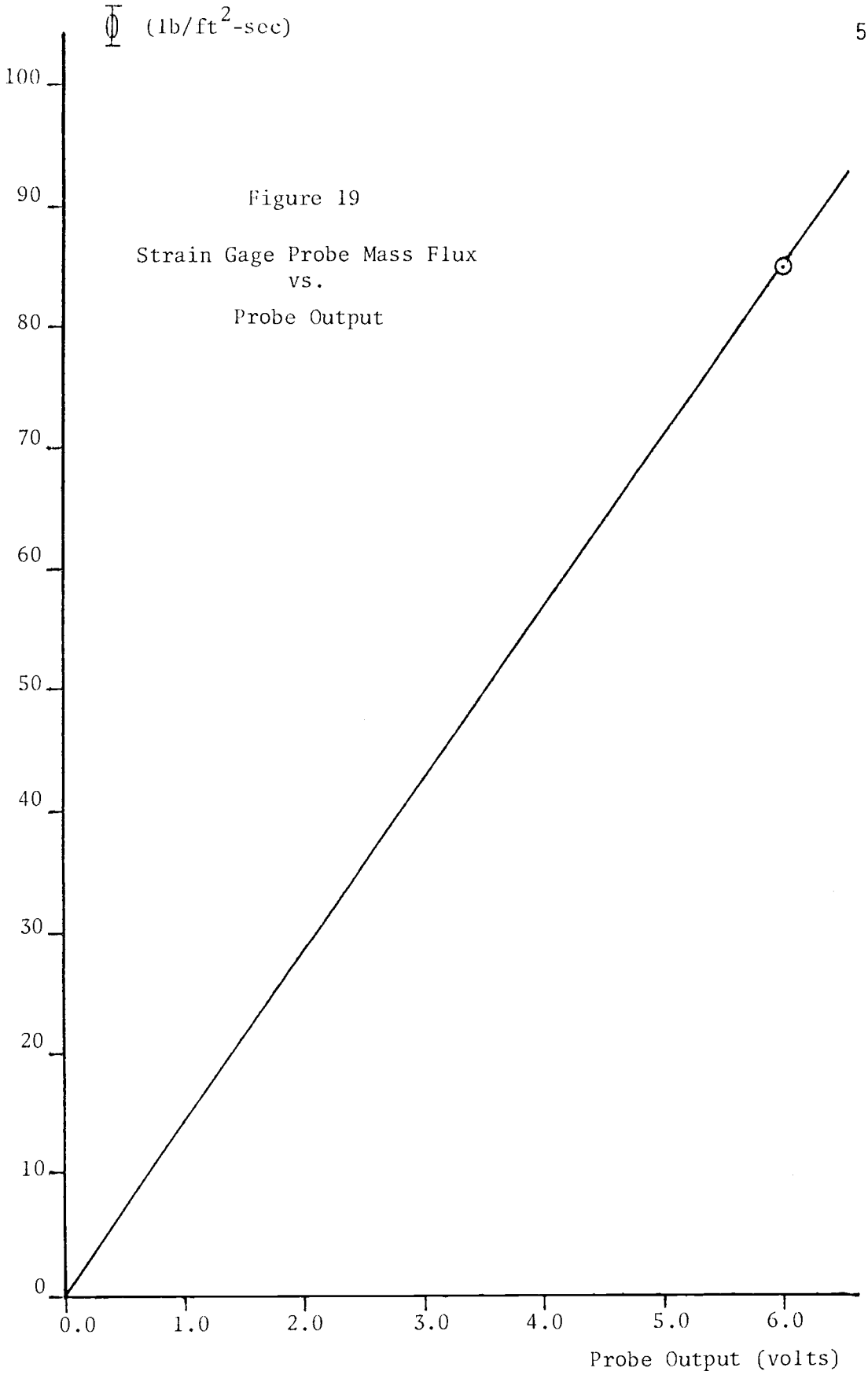

Figure 19

Strain Gage Probe Mass Flux
vs.
Probe Output

STRAIN GAGE PROBE DESIGN

The actual strain gage consisted of a 4.25 inch (10.8 cm) long, 3/16 inch (4.7 mm) diameter cantilever beam mounted into a circular plexiglass base unit (figures 20, 21 and 22). The base was designed so that it could be easily placed into and removed from a test section mounting device which is shown in figures 23, 24 and 25. The test section mounting device was designed so that it could be rotated 90° thus enabling the measurement of both horizontal and vertical solids movement without removing the probe from the bed for reorientation.

Plexiglass was chosen as a beam material because of its lower modulus of elasticity than metal. The beam diameter chosen was the smallest one which could be used without breaking off at the base while in the bubbling bed. The 4.25 inch (10.8 cm) beam length was selected since it was the longest one which could be used with the torque motor calibration technique and still be approximately 1 inch (2.54 cm) away from the bed walls.

Placement of the strain gages on the probe base and beam is shown in figures 20 and 21. The gages used were EA-06-031DE-120-LE strain gages manufactured by Micro-Measurements, Inc. Nominal gage resistance was 120 ohms with an excitating voltage of 0.1 volts being used to minimize resistance heating of the gage network. The gages required shielding from the destructive abrasion of the sand particles in the bed but the shielding must also not significantly affect the dynamics of the probe. Dow-Corning RTV 3140 silicone rubber was used to cover the gages. In addition, the silicone rubber

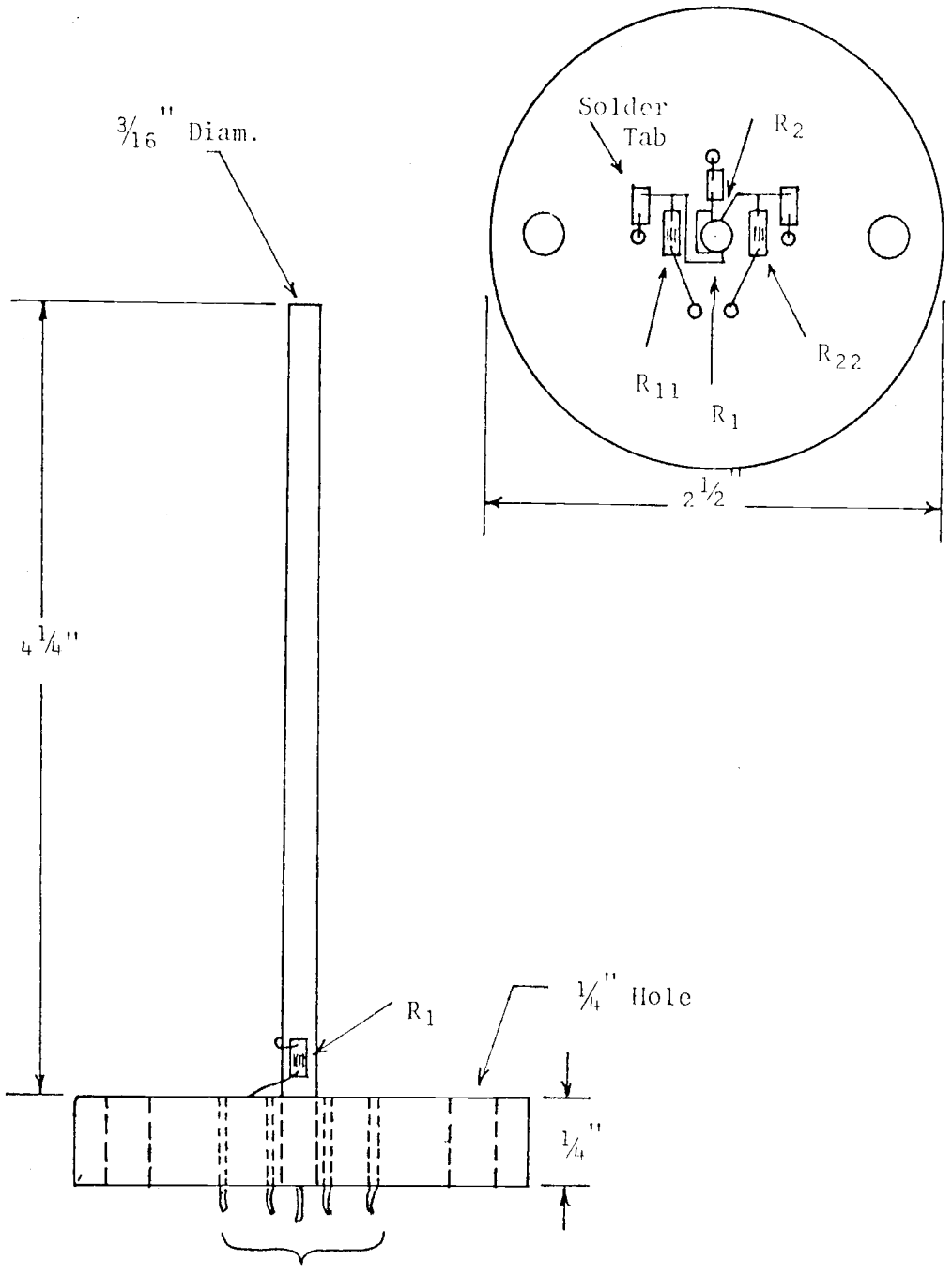

Figure 20 Strain Gage Probe Details

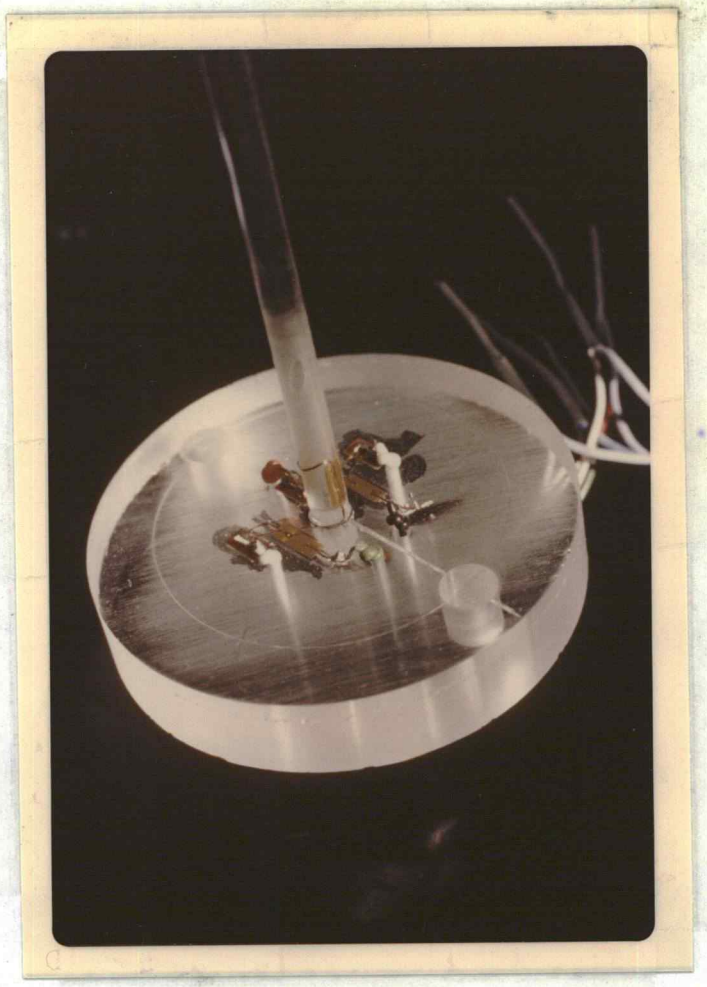

Figure 21 Close-up Photograph of the Strain Gage Placement

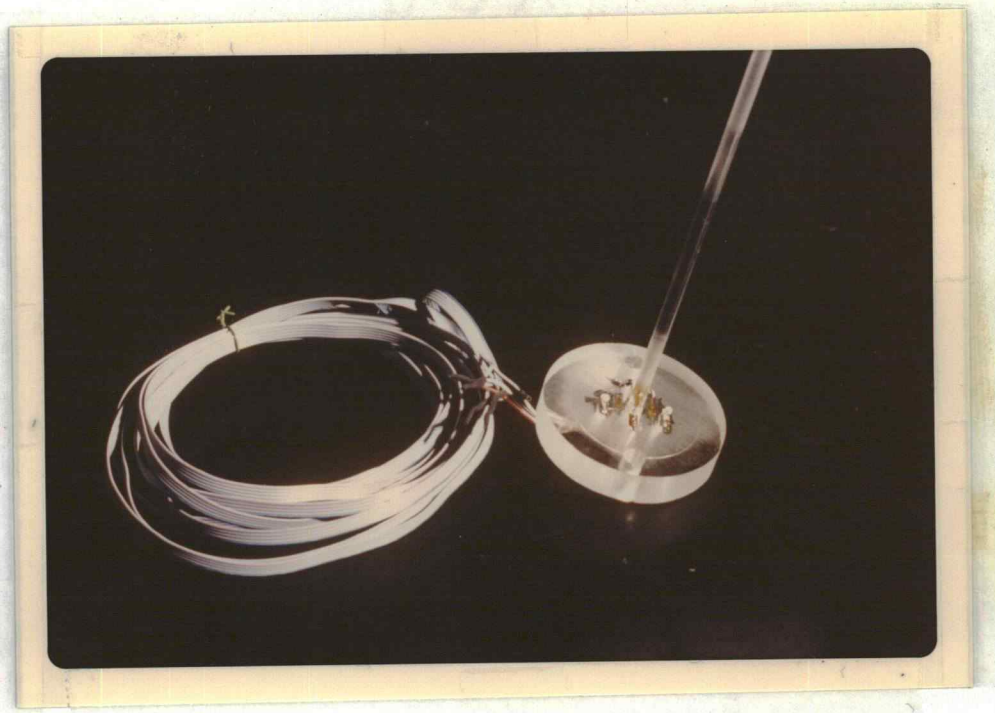

Figure 22 Photograph of the Strain Gage Probe

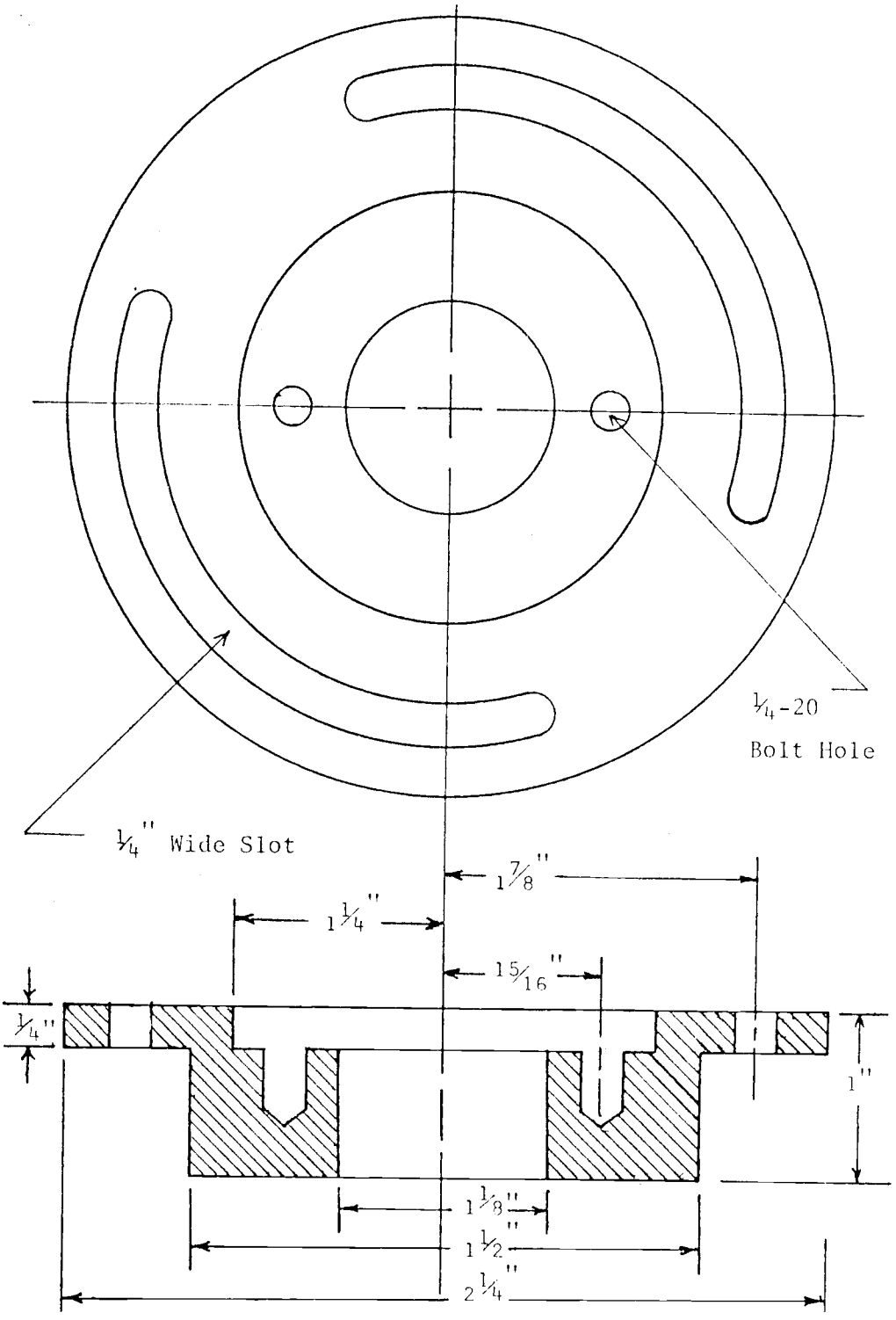

Figure 23 Strain Gage Probe Bed Mounting

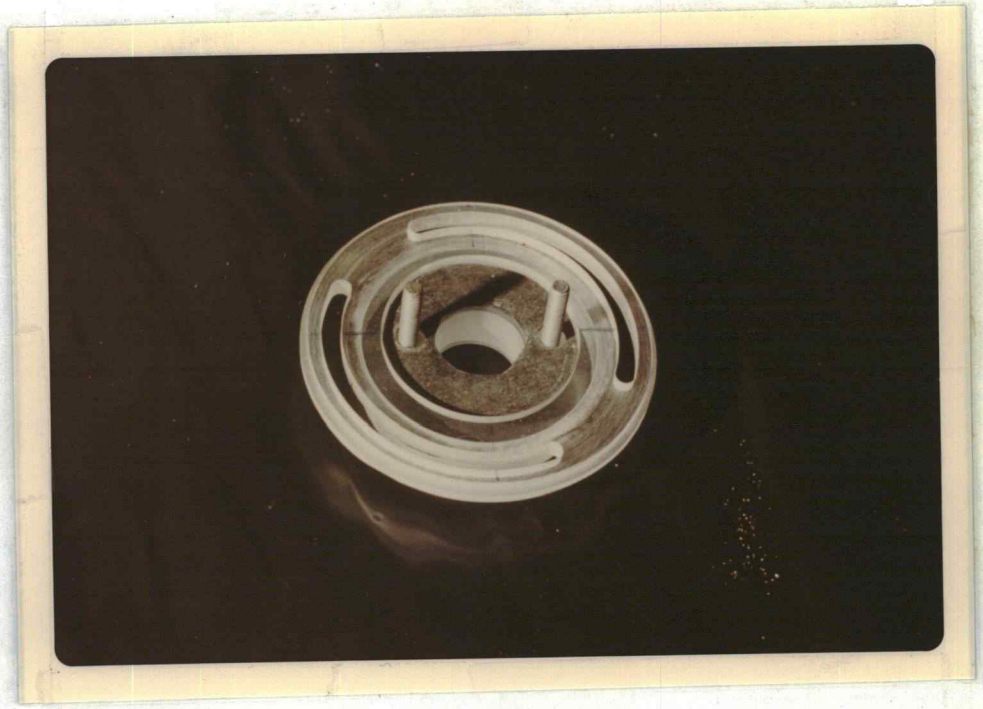

Figure 24 Photograph of the Strain Gage Probe Bed Mounting

Figure 25 Photograph of the Probe in its Bed Mounting

was free of any acetic acid which may have had corrosive effects on the gages and their wire leads.

STRAIN GAGE PROBE EXPERIMENTAL WORK

Planned Experimental Program

The original experimental program planned for the strain gage probes consisted of measuring both vertical and horizontal solids movement. Horizontal movement would be correlated in a manner similar to vertical movement; ie, by finding a J_h value for horizontal "turnover rates". Solids movement would be measured with tubes in the bed and without tubes in the bed. The probe and tube configurations are shown in figures 26, 27, 28 and 29. Four superficial fluidizing velocities were used: 1.3, 1.5, 1.75, and 2.0 U_{mf}. If there were found to be minor differences in J values at the lower U_o values, then air velocities of 2.5 and 3.0 U_{mf} were to also be investigated. Only one size distribution of sand with $\overline{d_p}$ of 0.96 mm (0.038 inch) was to be used for all runs. All settled bed heights were 11.5 inches (29.2 cm).

Experimental Results

Because of temperature induced output offset drift, immediately after each run at U_o, the bed was drained of solids and the offset value for zero torque was found for the static probe. This offset value would then be subtracted from the tape recorded probe output when replayed. It was found that just using the final offset and subtracting it from the averages would not work. By using only this method, there would often be indicated a net upward or downward flow for all of the probes, which was not possible.

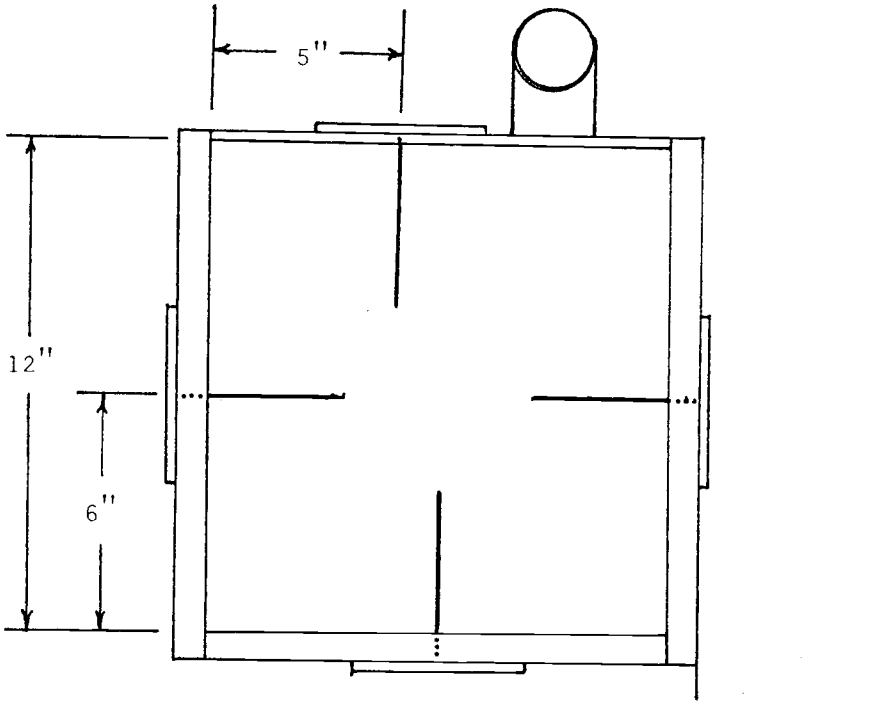

Top

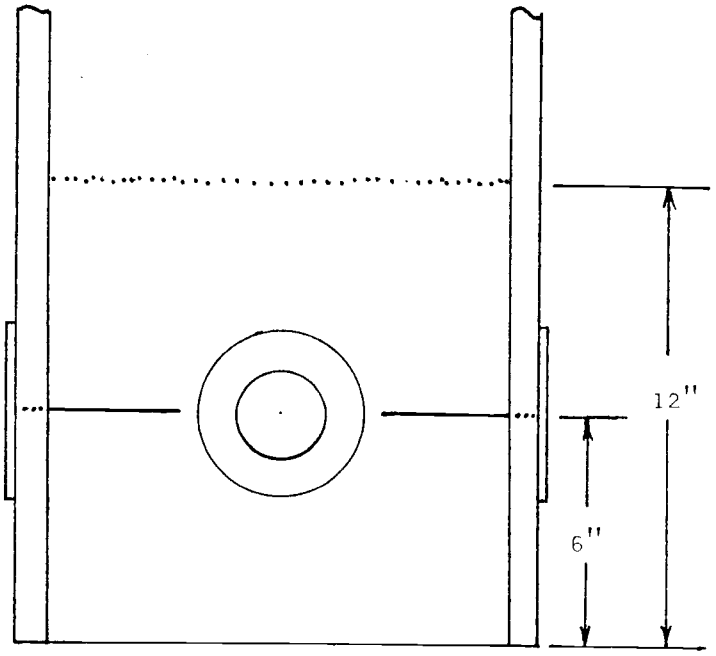

Side

Figure 26 Strain Gage Probe Location in the Small Bed

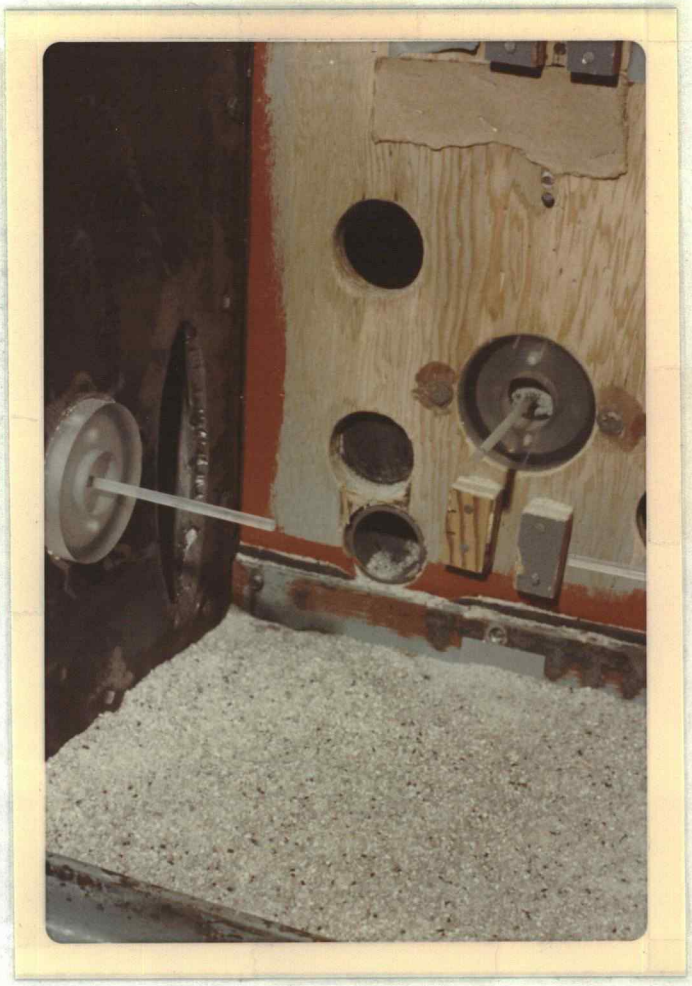

Figure 27 Photograph of the Strain Gage Probes in the Bed

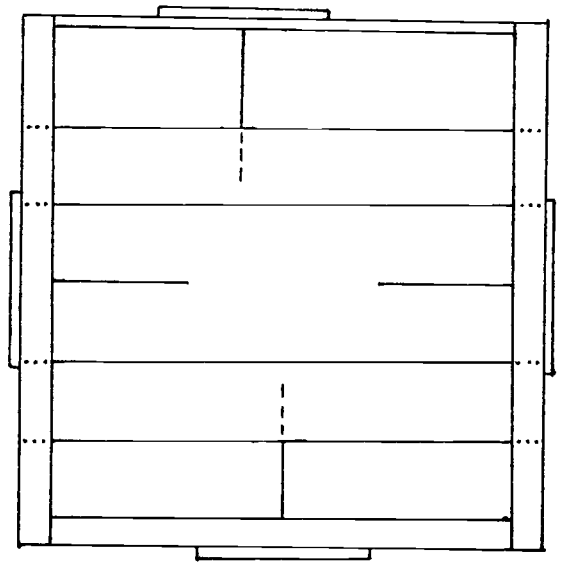

Top

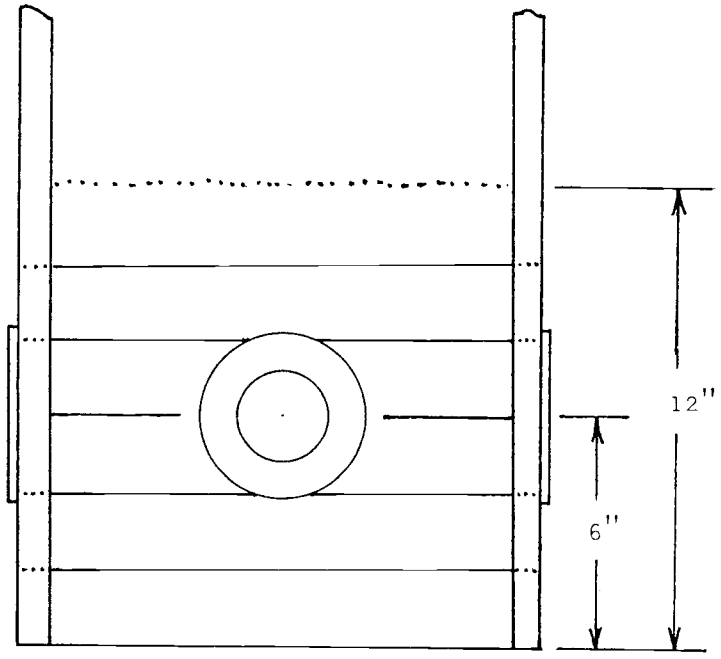

Side

Figure 28 Strain Gage Probe and Inductance Probe Tube Location in the Small Bed

Figure 29 Photograph of Strain Gage Probes and Inductance Probe Tubes in the Bed

When analyzing the experimental data, net flow past a probe was first found without rectifying the signal. This net flow was used as a preliminary check of the data. If the net flows past each probe were summed and found to be zero, one could then proceed and try to rectify the signals to find the upward and downward components of solids motion past each probe.

After it was found that static probe offset values would not yield reasonable net flow values past each probe, closer examination of the probe output suggested that there was a dynamic rest output level which was not the same as the static rest output level. Dynamic rest output level is intended to mean the zero torque output level in a bubbling bed where the probe is continuously deflecting. It is thought that the existence of a dynamic rest output level which is different from the static level may be due to two different mechanisms. First, it is possible that resistance heating of the strain gages which are mounted on plastic and sealed inside a silicone rubber shield may cause continuous temperature variations of the gages which are different than those of the static probes. These temperature variations then cause changes in gage resistance. It is possible that gage heating may cause local changes in the plastic beams modulus of elasticity which may be responsible for the changes in the probe zero torque level. Also, it may be possible that the stretching and relaxation of the probe beam is causing elastic heating and cooling at the location of the strain gages. This heating may then be responsible for the gage resistance changes due to temperature fluctuations of the gage substrate material. The

differences between dynamic and static rest output levels can be seen in figure 30.

The dynamic rest levels were found by expanding the output scale and the time scale of the strip chart recorder. An attempt was then made to find the "position" which the probe returned to most often before the output signal changed direction. This technique was moderately successful in that it yielded net mass fluxes that would sum to approximately zero. When the signal was rectified and filtered and the upward and downward average fluxes were summed, they did not yield the same net value as when the signal was filtered without rectification. This difficulty may be due to slight errors in the analog subtractor unit. Also, the fact that the filtered average flux doesn't remain constant makes it difficult to obtain completely consistent rectified and unrectified mass flux averages.

Offset drift and the magnitude of the offset when compared with the average mass flux obtained after the probe output is corrected for offset make the mass flux very sensitive to errors in offset values. Table A1 in the appendix illustrates this point where uncorrected average probe output signals, estimated offsets and net mass fluxes are listed. The offset signal ranged from 50 percent to 95 percent of the total average signal.

Calculation of J_v Values

Despite the errors that were present in the strain gage probe values of $\bar{\Phi}$, turnover rates were calculated for the cases of tubes present and absent from the bed. Tables A1, A2, A3, and A4 show the

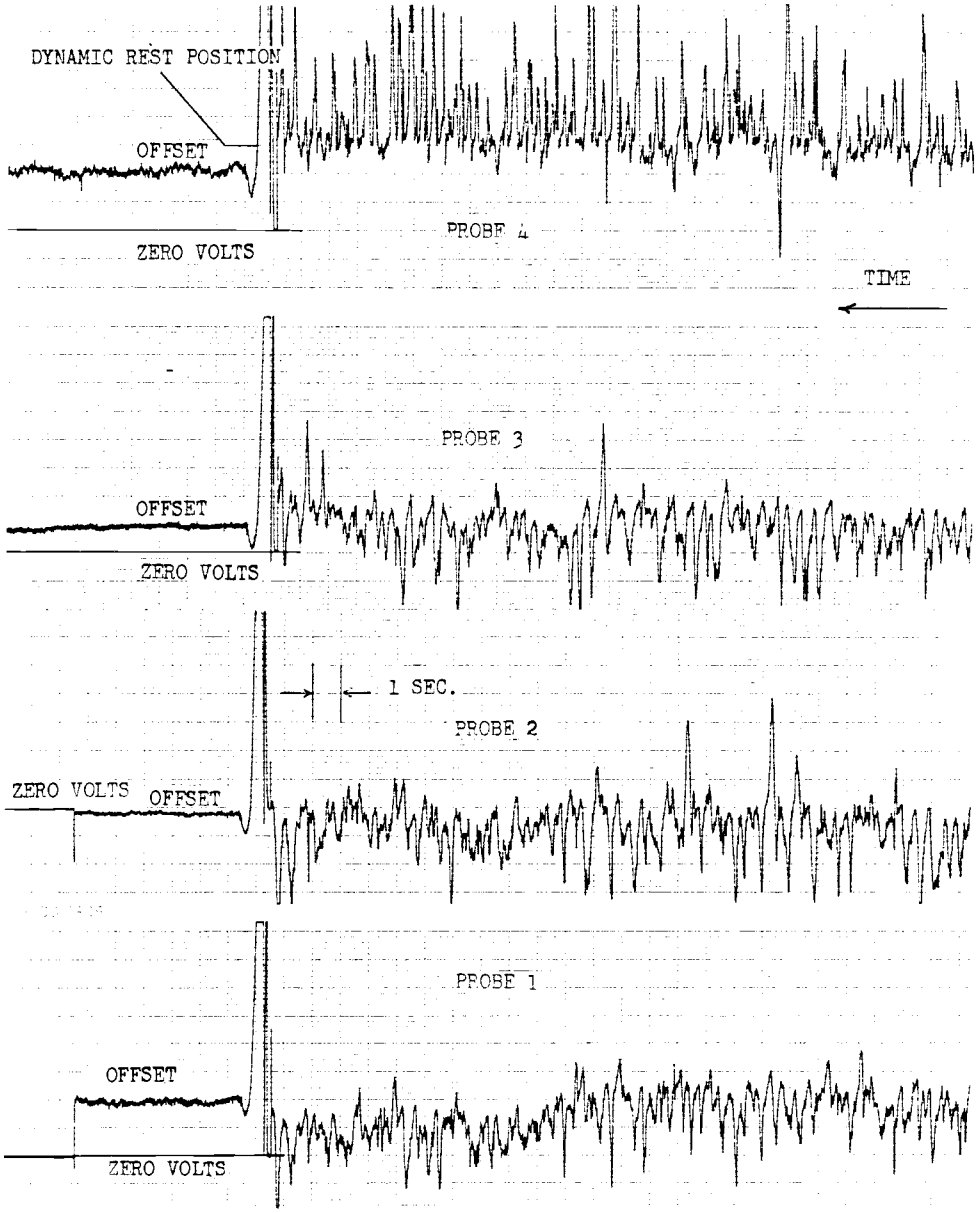

Figure 30 Sample Strain Gage Probe Output

probe output averages, the mass flux averages and the turnover values. Horizontal flow coefficients or J_h values weren't measured as a result of preliminary tests which showed that the horizontal probe output was very susceptible to vertical solids movement which caused a vertical deflection in the probe in addition to the horizontal deflection.

Figure 31 summarizes the results of the turnover measurement experiments. As was expected, the tube free bed had the consistently higher turnover values while the tube filled bed tended to obstruct the vertical movement of solids. The turnover values also are well within order of magnitude agreement with the observations of other investigators. The J_v values obtained by Geldart and Cranfield (9) range from 0.1-1.0 gm/cm^2-sec (0.205-2.05 lb/ft^2-sec) for U_o = 1.17-2.67 U_{mf} using 1-2 mm (0.039-0.079 inch) alumina particles. Considering that there were two completely different techniques used to measure the J_v values this agreement is remarkable.

Sample Calculation of J_v

$$U_o/U_{mf} = 2 \quad \text{(data from table A1)}$$

Probe	Average + Voltage	Average - Voltage
1	+ 0.08	- 0.07
2	+ 0.05	- 0.20
3	+ 0.17	- 0.04
4	+ 0.15	- 0.14

$$\bar{\Phi} = (\text{average voltage}) \cdot (14.19 \text{ lb/ft}^2\text{-sec-volt})$$

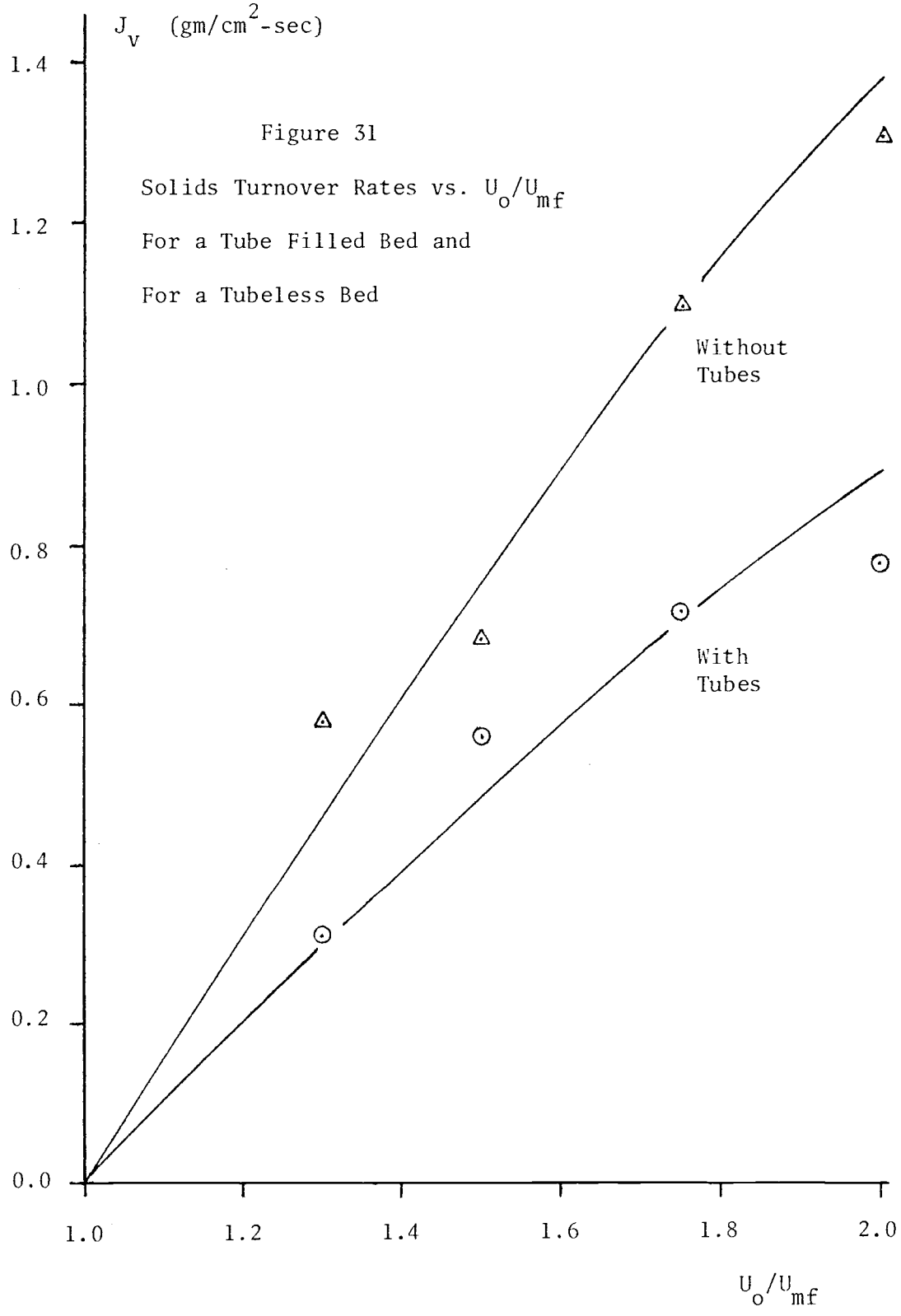

Figure 31

Solids Turnover Rates vs. U_o/U_{mf}

For a Tube Filled Bed and

For a Tubeless Bed

For probe 1, the average + voltage is + 0.08 volt

$$+\Phi_1 = (+\ 0.08\ \text{volt})\ (14.19\ \text{lb/ft}^2\text{-sec-volt})$$

$$= +\ 1.14\ \text{lb/ft}^2\text{-sec}$$

$$+J_v = \frac{1}{4} \sum_{j=1}^{4} + \Phi_j$$

$$+J_v = 0.25\ (1.14 + 0.71 + 2.41 + 2.13)$$

$$+J_v = (1.60\ \text{lb/ft}^2\text{-sec})\ (0.4887\ \frac{\text{gm/cm}^2}{\text{lb/ft}^2})$$

Hence: $J_v = +\ 0.78\ \text{gm/cm}^2\text{-sec}$

CONCLUSIONS AND RECOMMENDATIONS

It was concluded that because of the sensitivity of average mass flux values to offset errors and the fact that offset was difficult to precisely determine, the experimentally obtained mass flux values and turnover values obtained with the existing strain gage probe should only be regarded as estimates within an order of magnitude of the true mass flux values. Since such difficulty was involved in obtaining vertical mass fluxes (which are much larger than horizontal mass fluxes), horizontal flux values weren't measured.

For practical data taking, an instrument should be convenient and simple to use with a minimum of corrections which need to be made to the output signal. The offset and temperature caused offset drift make it difficult for the existing strain gage probe to fulfill the latter criterion. A redesign of the probe which would make it insensitive or less sensitive to temperature and hence reduce offset is necessary. Figure 32 represents such a redesign.

The new design would utilize a strip of spring steel with the wide area facing the direction of flow. Strain gages would then be mounted at the base of this beam. Since this beam will be made of metal, it will act as a much better heat sink than the existing probe. Any possibilities of elastic heating of the beam are eliminated by using metal instead of plastic. The beam should deflect enough to induce a measureable strain at the base yet the beam shouldn't deflect so much that solids will begin to slip past the

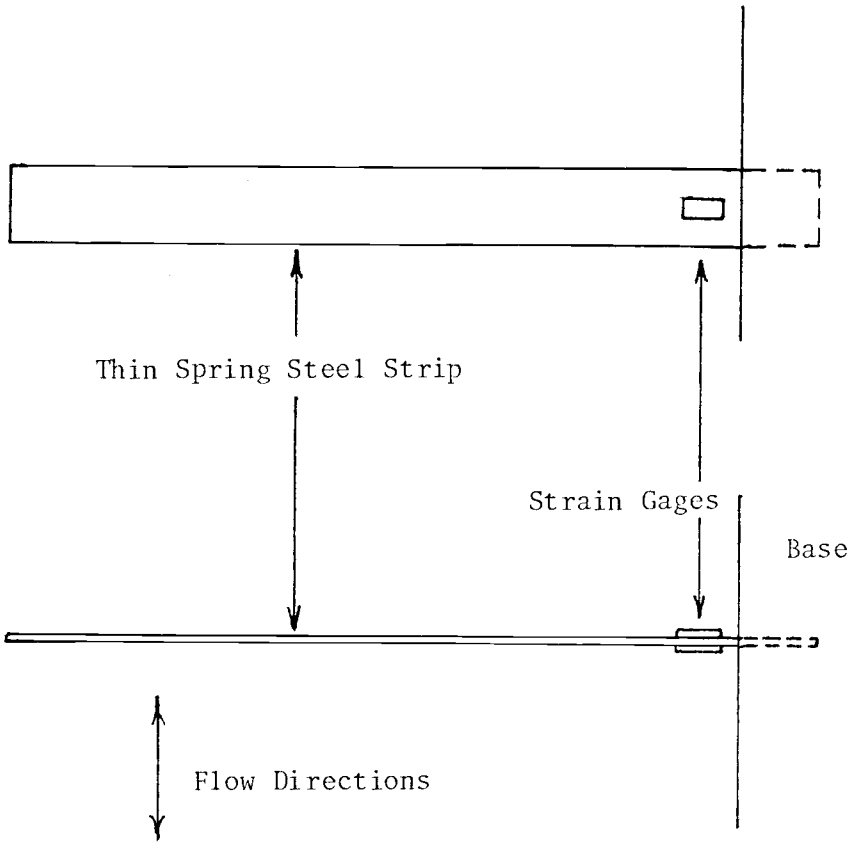

Figure 32 Redesigned Strain Gage Probe

end of the probe rather than slip around the sides. It is also possible that temperature compensating resistors won't be needed and that fixed value precision resistors can be used in the remainder of the bridge circuit.

Qualitatively, the strain gage probe was a success for the case of tubes both present and absent from the bed. Sections of the bed which were known to be poorly fluidized (ie; few bubbles through a given area per unit time) reflected this condition with a lower frequency of upward mass flux peaks and a lower peak amplitude than in the more vigorously fluidized regions. In order for more reliable quantitative measurements which reflect only bed behavior and not instrument errors, there must be a probe redesign as described above.

IV. THE INDUCTANCE PROBE METHOD FOR SOLIDS MOVEMENT MEASUREMENT

INTRODUCTORY COMMENTS

The inductance probe method was conceived of by Dr. Thomas Fitzgerald. The method utilizes a ferrite tracer which is detected by an inductor coil probe which is located inside of a dummy heat exchanger tube immersed in the fluidized bed. The coil is part of a bridge circuit which is initially in balance when no tracer is near the probe. When ferrite is near the probe, its inductance is reduced and the bridge goes out of inductive balance. The resulting output signal is linear with respect to ferrite concentration.

The inductance probes will yield transient tracer concentration curves in response to a tracer pulse released in a given region of the bed. When the method is used in conjunction with the Chang flow model, the continuous tracer curves for each probe will be discretized and manipulated according to the analysis procedure to be outlined. Ultimately, the analysis will yield vertical solids turnover rates and horizontal mass flow coefficients analogous with the turnover rates. These turnover rates will be compared with those obtained by the strain gage probe method.

THEORETICAL CONSIDERATIONS

Calculating Turnover Values Using the Chang Flow Model

The essence of the Chang model is a Markov transition probability matrix which represents the fraction of material which will flow from one compartment into all other compartments during a time interval Δ t. In order for the model to be useful, whatever flow pattern exists within the bed must be stationary in time. In terms of discrete time notation, the tracer material balance is of the following form for a closed, non-flow system:

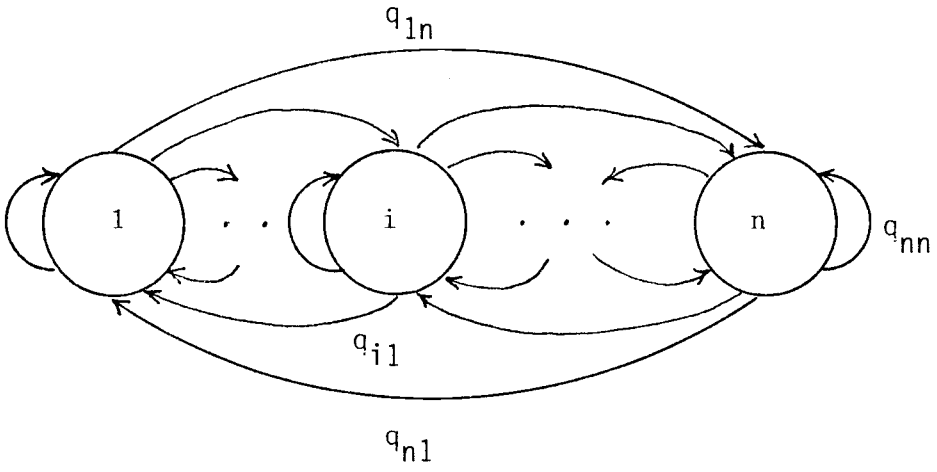

$$(7)\quad V_j\, c_j(t+\Delta t) = \sum_{i=1}^{n} q_{ij}\, \Delta t\, c_i(t)$$

or

$$c_j(t+\Delta t) = \sum_{i=1}^{n} \frac{q_{ij}\, \Delta t\, c_i(t)}{V_j}$$

(8) Define $$p_{ij} = \frac{q_{ij}\,\Delta t}{V_j}$$

Hence, $$c_j(t+\Delta t) = \sum_{i=1}^{n} p_{ij}\, c_i(t)$$

Generalizing for the entire network:

$$c_1(t+\Delta t) = \sum_{i=1}^{n} p_{i1} c_i(t)$$

$$\vdots$$

$$c_n(t+\Delta t) = \sum_{i=1}^{n} p_{in} c_i(t)$$

Condensing into matrix notation:

$$(9)\quad \left[c_1, c_2, .., c_n\right]_{t+\Delta t} = \left[c_1, c_2, .., c_n\right]_t \begin{bmatrix} p_{11} & \cdots & p_{1n} \\ \vdots & & \vdots \\ p_{n1} & \cdots & p_{nn} \end{bmatrix}$$

Where $c_i(t)$ = Tracer concentration in compartment i at time t

V_j = Volume of compartment j

Δt = The time interval over which the discrete time material balance is being made

q_{ij} = The volumetric flow rate of material from compartment i into compartment j

p_{ij} = The fraction of material which goes from compartment i into compartment j

n = The number of probes used to measure concentrations in the n compartments.

Further condensing into matrix notation:

$$(10)\quad C(t+\Delta t) = C(t)\ P$$

or

$$C(1) = C(0)\ P$$
$$C(2) = C(0)\ P^2$$
$$\vdots$$
$$C(n) = C(0)\ P^n$$

Where $C(t) = \left[c_1(t), c_2(t), \ldots, c_n(t)\right]$

As a consequence of equation (10), etc. the P matrix is found as follows:

$$(11)\quad \begin{bmatrix} C(1) \\ C(2) \\ \vdots \\ C(n) \end{bmatrix} = \begin{bmatrix} C(0) \\ C(1) \\ \vdots \\ C(n-1) \end{bmatrix} \begin{bmatrix} P \end{bmatrix}$$

Hence

$$(12)\quad P = \begin{bmatrix} C(0) \\ C(1) \\ \vdots \\ C(n) \end{bmatrix}^{-1} \begin{bmatrix} C(1) \\ C(2) \\ \vdots \\ C(n-1) \end{bmatrix}$$

The Two Compartment Model

For the case of a two compartment model which was to have been used to calculate turnover rates, the data analysis procedure is simper. Figure 33 shows the two compartment model being used.

Given concentration data:

$$\begin{bmatrix} c_{01} & c_{02} \\ c_{11} & c_{12} \\ \cdot & \cdot \\ \cdot & \cdot \\ c_{n1} & c_{n2} \end{bmatrix}$$

Where $c_{tj} = c_j(t)$ the concentration of tracer in compartment j at time t. $c_j(t)$ is obtained by averaging the tracer concentrations read by the 2 probes within each compartment.

We have:

$$\begin{bmatrix} c_{11} & c_{12} \end{bmatrix} = \begin{bmatrix} c_{01} & c_{02} \end{bmatrix} \begin{bmatrix} P_{11} & P_{12} \\ P_{21} & P_{22} \end{bmatrix}$$

Since the columns of P must add to 1 for a closed system, $p_{11} = 1-p_{21}$, etc:

$$(13) \quad \begin{bmatrix} c_{11} & c_{12} \end{bmatrix} = \begin{bmatrix} c_{01} & c_{02} \end{bmatrix} \begin{bmatrix} 1-p_{21} & p_{12} \\ p_{21} & 1-p_{12} \end{bmatrix}$$

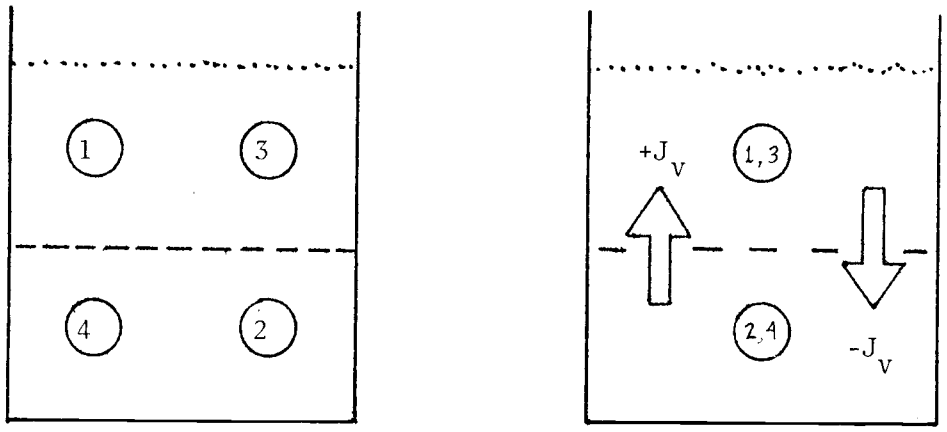

Vertical Solids Movement

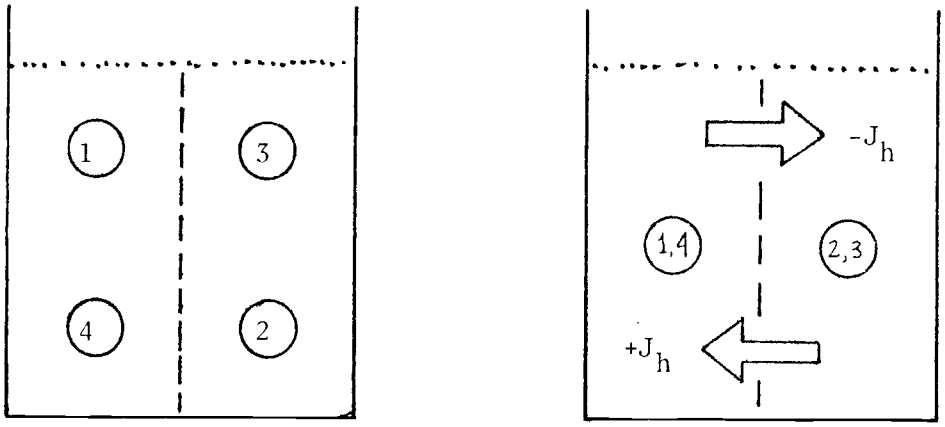

Horizontal Solids Movement

Figure 33 The Compartmental Models Being Used To Calculate J_v and J_h

Multiplying out the matrices:

$$c_{11} - c_{01} = p_{21}(c_{02} - c_{01})$$

$$c_{12} - c_{02} = p_{12}(c_{01} \quad c_{02})$$

In general:

$$(14) \quad P_{21} = \left(\frac{c_{t1} - c_{t-1,1}}{c_{t-1,2} - c_{t-1,1}}\right)$$

$$(15) \quad P_{12} = -\left(\frac{c_{t2} - c_{t-1,2}}{c_{t-1,2} - c_{t-1,1}}\right)$$

Based on the above two equations, a record of p_{12} and p_{21} values can be calculated:

$$(p_{12})_{t=1} \quad (p_{21})_{t=1}$$

$$(p_{12})_{t=2} \quad (p_{21})_{t=2}$$

$$\vdots \qquad \vdots$$

$$(p_{12})_{t=k} \quad (p_{21})_{t=k}$$

for statistical reasons, k should be large

The p_{ij} values which best fit the experimental data are simply the mean values obtained for each record. Once the p_{ij} values are known, the J values must be found. In order to find the J values, q_{ij}, the intercompartmental volumetric flow rates must be found. But before q_{ij} can be found, the V_j values or compartmental volumes must be first determined.

For the non-flow system it is known (4) that:

$$(16) \quad \sum_{j=1}^{n} p_{ij} V_j = V_i$$

Generalizing into matrix notation yields:

$$(17) \quad [P] \begin{bmatrix} V_1 \\ V_2 \\ . \\ . \\ V_n \end{bmatrix} = \begin{bmatrix} V_1 \\ V_2 \\ . \\ . \\ V_n \end{bmatrix}$$

Or:

$$[\,0\,] = [P - I] \begin{bmatrix} V_1 \\ V_2 \\ . \\ . \\ V_n \end{bmatrix}$$

For the case of a closed, non-flow system the P - I matrix is singular and cannot be solved for the V_i values directly. What is done to remedy the difficulty is to replace the last line of the compartment volume equation (17) by the equation:

$$(18) \quad V_{total} = V_1 + V_2 + \ldots + V_n$$

Where V_{total} is known from the particular vessel being considered. Equation (17) now becomes:

$$(19) \quad \begin{bmatrix} P_{11} & \cdots & p_{1n} \\ . & & . \\ . & & . \\ p_{n-1,1} & & p_{n-1,n} \\ 1 & \cdots & 1 \end{bmatrix} \begin{bmatrix} V_1 \\ . \\ . \\ V_n \end{bmatrix} = \begin{bmatrix} V_1 \\ . \\ . \\ V_{n-1} \\ V_{total} \end{bmatrix}$$

If the V_i values are divided by V_{total} and replaced by f_i and the p_{ij} matrix is condensed, we obtain:

$$(20)\quad \begin{bmatrix} p_{11}-1 & p_{12} & \cdot\cdot & p_{1n} \\ p_{21} & p_{22}-1 & \cdot & p_{2n} \\ \cdot & \cdot & & \cdot \\ \cdot & \cdot & & \cdot \\ p_{n-1,1} & \cdot p_{n-1,\,n-1} & & p_{n-1,n} \\ 1 & \cdot\ \cdot\ \cdot & 1 & 1 \end{bmatrix} \begin{bmatrix} f_1 \\ f_2 \\ \cdot \\ \cdot \\ f_{n-1} \\ f_n \end{bmatrix} = \begin{bmatrix} 0 \\ 0 \\ \cdot \\ \cdot \\ 0 \\ 1 \end{bmatrix}$$

Or:

$$(21)\quad \begin{bmatrix} [P - I]_{nxn-1} \\ \text{-----} \\ [1\ .\ 1]_{nx1} \end{bmatrix}_{nxn} \quad [f]_{1xn} = \begin{bmatrix} 0 \\ 0 \\ \cdot \\ \cdot \\ \cdot \\ 1 \end{bmatrix}_{1xn}$$

$[f]$ can now be found by inverting the modified $[P - I]$ matrix and multiplying it by the $[0\ 0\ .\ .\ 1]$ column vector.

For the two compartment model, the analysis reduces to:

$$(22)\quad \begin{bmatrix} f_1 \\ f_2 \end{bmatrix} = \begin{bmatrix} p_{11}-1 & p_{12} \\ 1 & 1 \end{bmatrix}^{-1} \begin{bmatrix} 0 \\ 1 \end{bmatrix}$$

Since V_{total} is known, V_1 and V_2 can be found from the f_i values.

Hence, q_{12} and q_{21} can be found using:

$$q_{ij} = \frac{p_{ij} V_j}{\Delta t} \qquad \text{(volume/time)}$$

If Δt is taken sufficiently small, q_{ij} for the discrete time model will be very nearly the same value as the continuous time q_{ij} value. For the case of two vertical or horizontal compartments 1 and 2:

$$(23) \quad J_v \text{ or } J_h = \frac{(q_{12})_{v \text{ or } h} \cdot \rho_{mf}}{A} \quad \text{(mass/area-time)}$$

Where A = the area across which flow is occurring.

ρ_{mf} = the emulsion phase density at U_{mf}.

The above values of J_v and J_h will then be compared with the J values obtained with the strain gage probe.

DESIGN OF INDUCTANCE PROBE AND CIRCUIT

The prototype probe detector circuit is shown in figure 34. The unique aspect of this detector system is its insensitivity to resistance changes in the detector coil due to self heating effects. The insensitivity is achieved by using a sinusoidal bridge driving voltage then multiplying the bridge output by this driving voltage and averaging the product. The resistive component of the bridge output voltage is 90° out of phase with the driving voltage and it is known that the average product of two sinusoids which are 90° out of phase with each other, is zero. Hence, when the bridge is inductively balanced (no ferrite near), the circuit output is zero. When the bridge is out of balance, the circuit output is nonzero and is due only to pure inductance changes in the probe coil. Shown also in figure 34 is the phasor representation of the driving voltage, and the resistive and inductive voltage components at various points in the circuit.

A brief mathematical analysis of the circuit follows. As represented in the phasor diagrams in figure 34, the input to the multiplier unit is:

$$v_d = V_d \sin(\omega t)$$

$$v_r + v_l = V_r \sin(\omega t + \frac{\pi}{2}) + V_l \sin(\omega t)$$

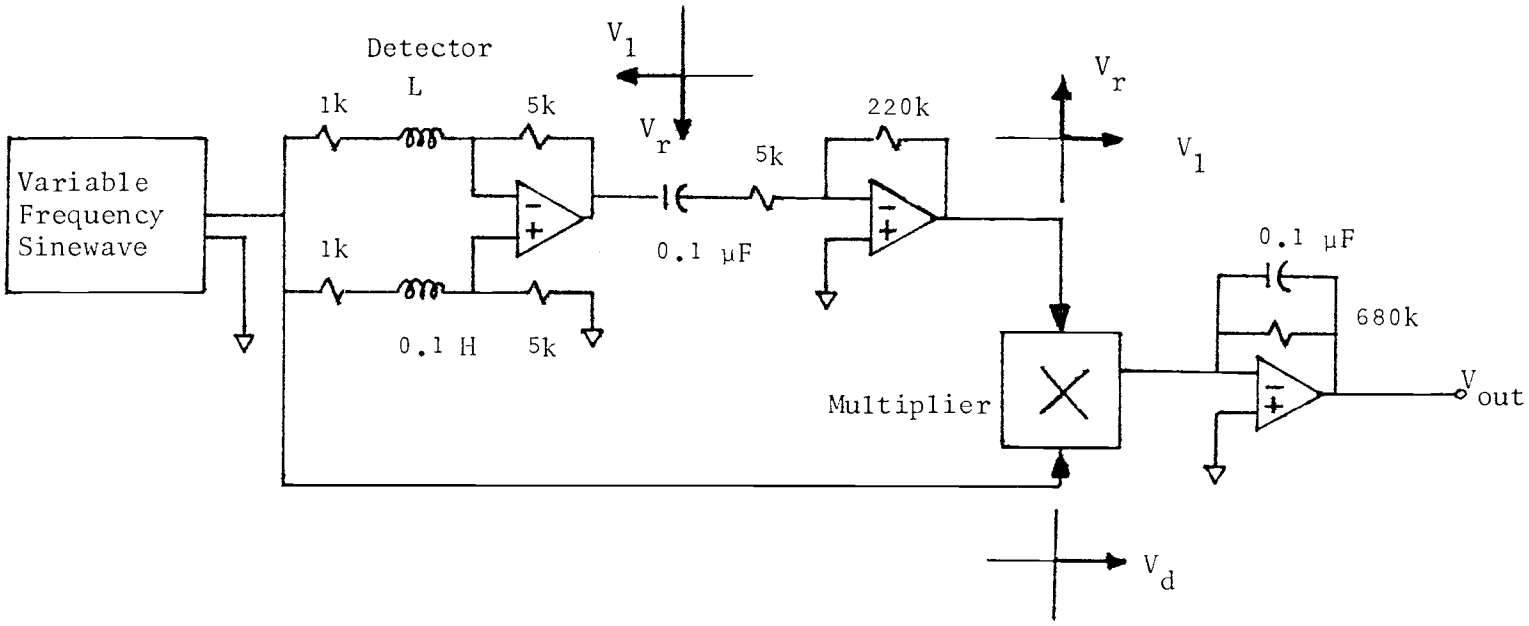

Figure 34 Simplified Inductance Probe Detection Circuit

The output of the averaging filter is:

$$v_{out} = \overline{V_d \sin(\omega t)\left[V_r \sin(\omega t + \frac{\pi}{2}) + V_1 \sin(\omega t)\right]}$$

$$= \left[\overline{V_d V_r \sin(\omega t)\sin(\omega t + \frac{\pi}{2})}\right] + \left[\overline{V_d V_1 \sin^2(\omega t)}\right]$$

$$v_{out} = V_1 \left[\overline{V_d \sin^2(\omega t)}\right]$$

constant

Hence, the output voltage is a linear function of V_1 which is itself a linear function of ferrite tracer concentration near the detector coil.

The inductance probe itself was made of a 1.65 inch (4.19 cm) OD plastic PVC pipe upon which approximately 1200 turns of #30 enameled wire was wrapped into a 3 inch (7.6 cm) long coil. The coil tube was then filled with seven, 1/2 inch (1.27 cm) diameter sections of ferrite material. The inductor was then trimmed to an inductance of 0.1 Henry by removing coil turns as necessary. The wire coil was then coated with a layer of Varathane plastic and then was wrapped in tape for protection. Figure 35 shows coil and ferrite coil core section details.

The ferrite tracer material used were small "donuts" of off-grade ferrite cores used in computer magnetic core memories. Bulk density of the ferrite was approximately 4 g/cm^3 (252 $\frac{lb}{ft^3}$). The

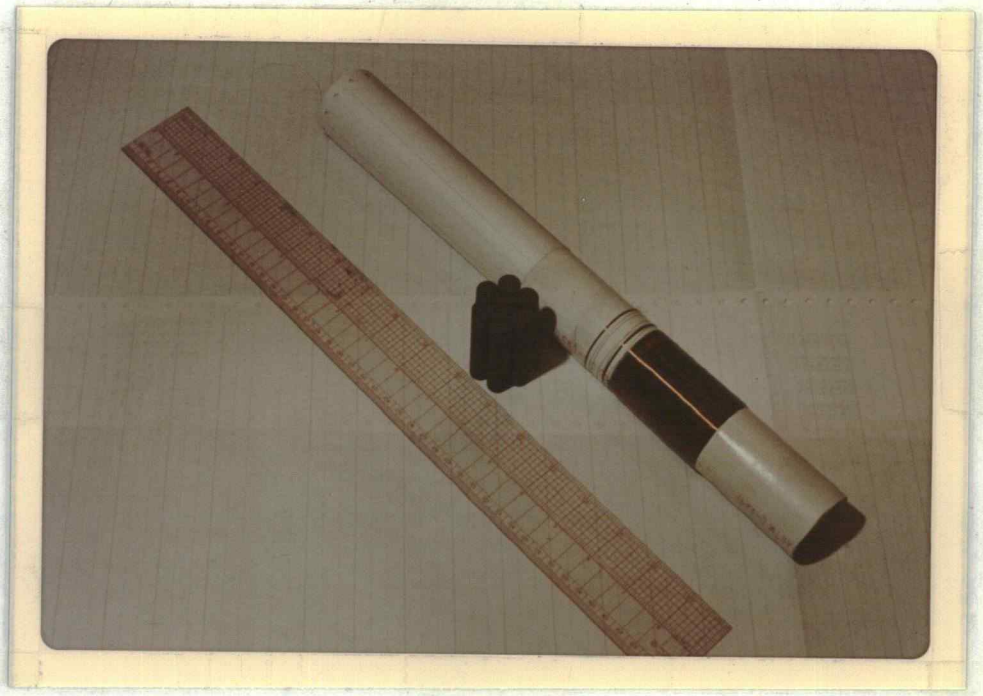

Figure 35 Photograph of the Probe Coil and the Coil Core

cores were made of what is referred to as a "soft" magnetic material. That is, there is little hysteresis loss or residual magnetism left in the material when an applied magnetic field is removed. Hence, when the ferrite comes near the inductance probe, it will only cause a change in the inductance and won't introduce a resistive component into the probe due to hysteresis losses. Shown below is an illustration of the ferrite core or bead:

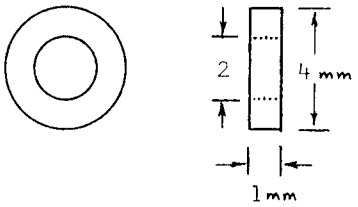

The detector probe and amplifier were calibrated by placing the detector coil inside of a fiberglass tube which was immersed in a mixture of ferrite and sand in a small cardboard barrel. The ferrite and sand had been well mixed and the quantities of each were measured prior to mixing. Probe gain was adjusted so that there was an output swing of approximately 1 volt/volume percent of ferrite. Because of the slightly different frequencies used for each probe circuit, the calibration factor varied from probe to probe. It was also found to be more convenient to express tracer concentration in lb of ferrite/ft^3 of total volume, so the probes were calibrated in these units. Calibration results for the probes were as follows:

Probe	lb ferrite/ft^3-volt	(kg/m^3-volt)
1	1.506	(24.15)
2	1.004	(16.10)
3	1.146	(18.37)
4	1.023	(16.40)

INDUCTANCE PROBE EXPERIMENTAL WORK

Experimental Strategy

With the inductance probe method, 2 flow parameters were to be found: J_v, the vertical solids turnover rate and J_h, the horizontal solids flow coefficient, J_v was to be determined by using two vertical compartments:

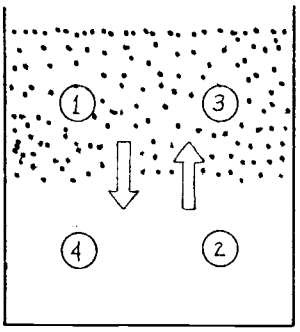

Tracer would be released into the top compartment so that it would land in a sheet across the upper surface of the bed. At this point, the tracer would begin to vertically mix until the tracer was uniformly distributed. J_v would be determined as outlined in the theoretical discussion section.

In a like manner, the horizontal flow coefficient or mass flux, J_h would be determined. The bed would be represented as consisting of two horizontal compartments:

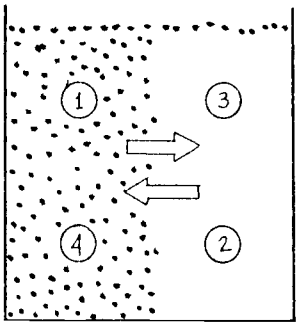

The two compartments would be separated by a removable partition or shutter. In one compartment there would be well mixed tracer and in the adjacent compartment there would be little or no tracer. When the partition is removed, tracer would begin to mix horizontally until there was a uniform tracer concentration through the bed.

Initially it was hoped to obtain J_v and J_h values at U_o values of 1.3, 1.5, 1.75, and 2.0 U_{mf} but at 1.3 through 2.0 U_{mf}, the bed didn't fluidize uniformly. For these values, it was found that the tracer wouldn't mix thoroughly even after periods of high agitation. The details of this problem are described in the mixing and slumping studies in the section on experimental results.

Experimental Setup

The probe arrangement used in the inductance probe experiments is shown in figure 36. The bed was divided into four regions, at the center of which was located the coil. Each region measured 6 inches (15.2 cm) high, 6 inches (15.2 cm) wide and 12 inches (30.5 cm) long. The dummy heat exchanger tubes consisted of 1-15/16 inch (4.9 cm) OD fiberglass piping into which are inserted the inductance probes. The inductance probes are arranged in the bed the way that they are so that there won't be any interaction between the probes which have driving frequencies near those of the other probes. When there is interaction, beating of the frequencies occurs and causes distortion of the probe circuit output signal.

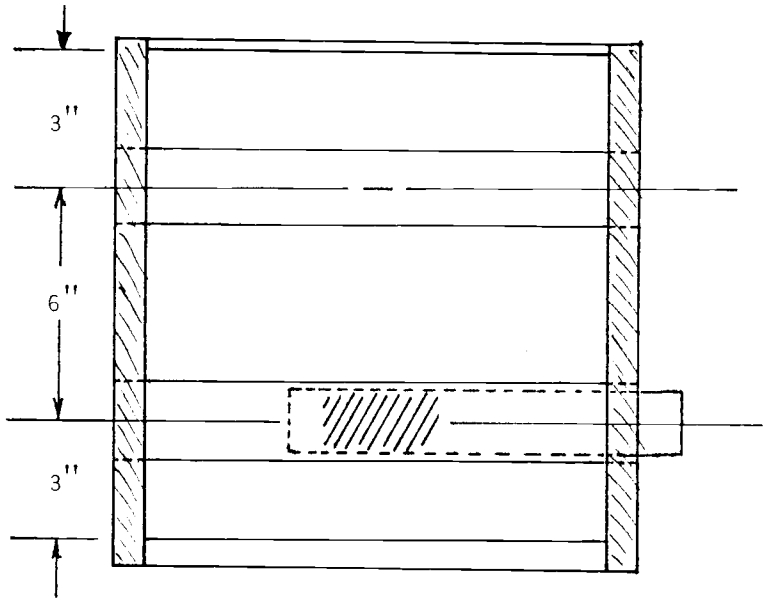

Top

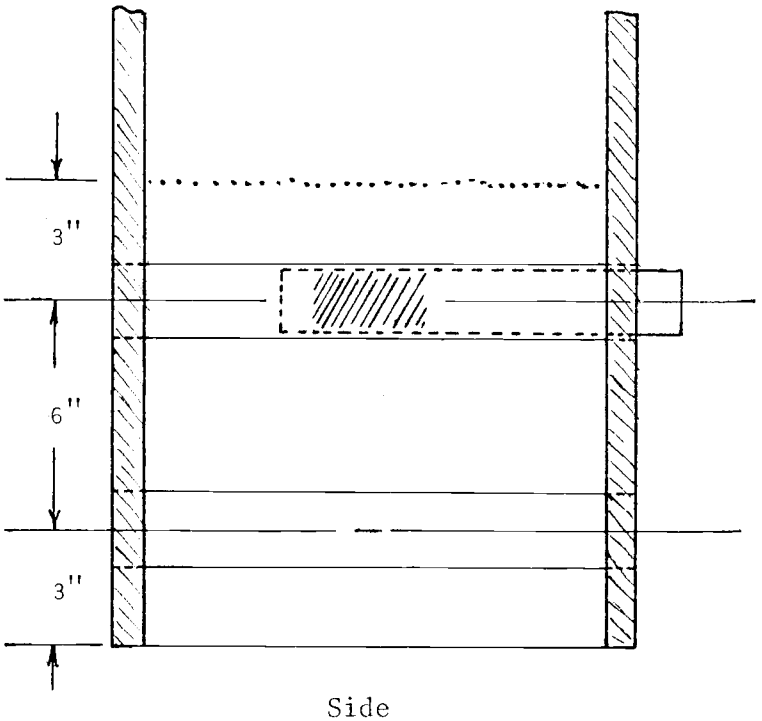

Side

Figure 36 Inductance Probe Location in the Small Bed

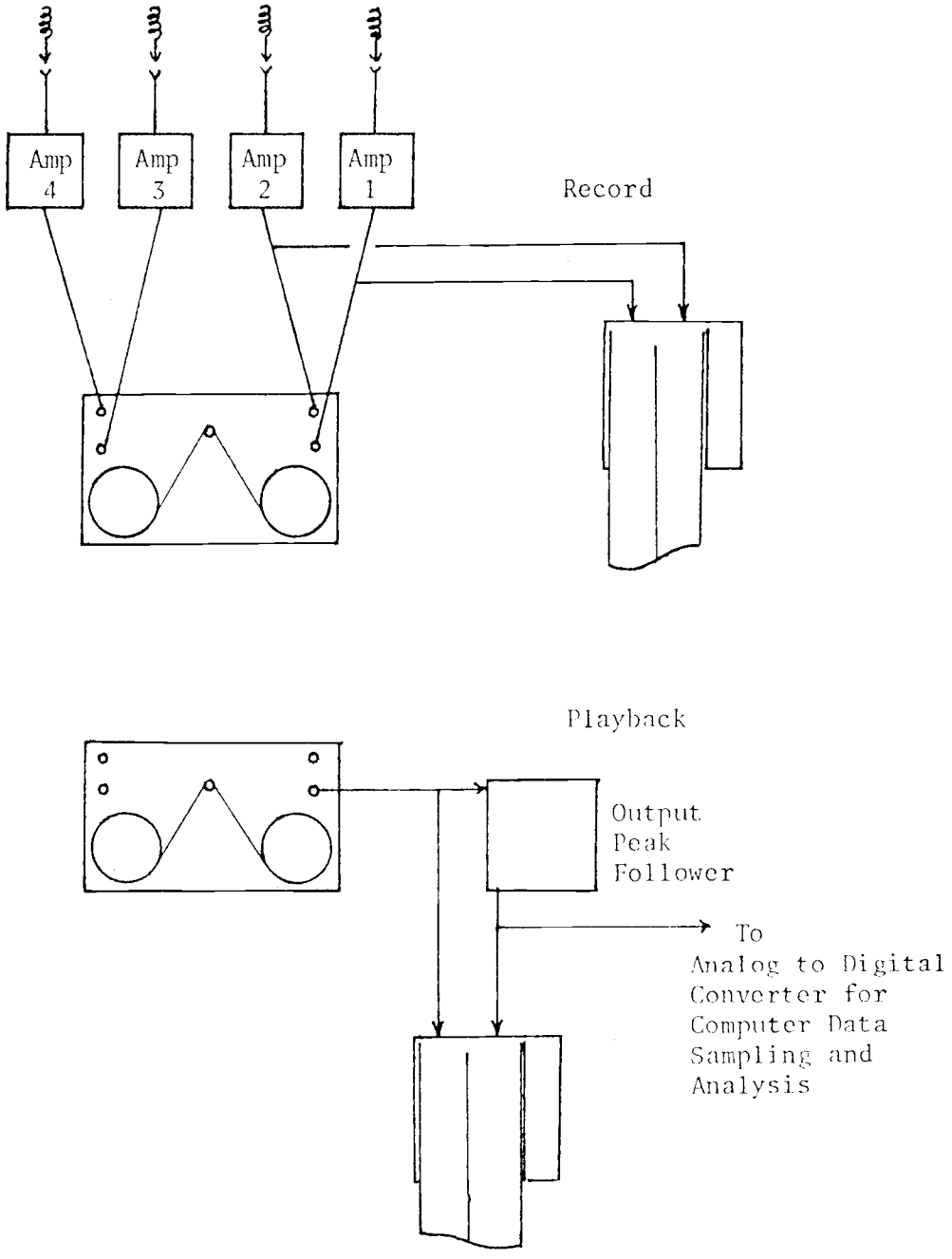

Figure 37 Inductance Probe Data Recording and Playback

Mixing and Slumping Studies

For the induction probe and ferrite tracer method, it was initially assumed that the ferrite core material used as the tracer would fluidize and follow the behavior of the sand particles. After making preliminary runs which involved the horizontal movement of ferrite, it was found that at low air velocities (1 - 2 U_{mf}) there would be an apparent segregation of tracer which was indicated by the inductance probes. The probes were carefully checked and recalibrated for a standard or reference tracer concentration and a series of mixing and slumping studies were carried out.

The purpose of this series of mixing studies was to see how well the bed would mix the ferrite beads and how much the probe measured "well mixed" concentrations differed from the theoretical well mixed tracer concentrations for each run. Ideally, each probe should measure the same ferrite concentration and the concentration which is measured should be the same as the theoretical value which is calculated for each batch of tracer put into a known volume of bed solids.

Assuming that the probes are properly calibrated, any appreciable deviations from the theoretical tracer concentration may indicate the following: The ferrite beads aren't behaving like an ideal tracer; that is, the ferrite isn't moving around in the bed in the same manner as the sand. Local effects in the bed may be responsible for poor mixing such as a poor distributor plate which leaves parts

of the bed relatively starved for fluidizing air and has fewer or no bubbles passing upward.

The bed was mixed for 30 seconds and the bed was slumped or rapidly defluidized by cutting off the bed air supply. Two air velocities were used for mixing the bed: 1.75 and 3.0 U_{mf}. For the first set of runs, whole or intact ferrite cores or beads were used. Figure 38 summarizes the results of this run. Probes for compartment (1,4) read consistently higher concentration values than the probes in the compartment near the steel wall section of the bed. Under each U_o value, the repeatibility of concentrations for each probe varied with a normalized standard deviation (std.dev/mean) of as much as 18 percent.

It was thought that at 3 U_{mf}, the solids would be well mixed. If this were the case, then there was something else which was causing otherwise well calibrated probes to give erroneous readings when placed in the bed. The most likely explanation would be that there was an interaction between probes 2 and 3 and possibly probe 4 which were near either the steel of the one bed wall or near the steel of the bed distributor plate. This interaction was causing the magnetic fields set up by the probes to be "stretched out" toward the bed wall which would cause a decrease in the sensitivity of the probes to a given amount of ferrite.

Based on the results of this first mixing study, there was thought to be two possible explanations for the variations in tracer concentrations: there is actually poor mixing of the tracer because

of its size or density and there is also decreased probe sensitivity near the steel wall of the bed. The next run was done to see whether there was poor mixing of tracer due to its size. The ferrite cores were broken up so that they had the following mesh size distribution:

-12 +14 : 91% by weight

-14 +20 : 9%

Most of these particles were half crescent shaped and hence were still quite large. The probes were still in the same position as in the first mixing run. Figure 39 a & b summarizes the results of this run.

The next run had the probes rearranged so that what was once on one side of the bed was on the opposite side and what was once on top is now on bottom. Figure 39 c summarizes the results. Comparing the results of this run and the previous run, it is seen that there is still a trend for the probes near the steel wall to read lower values than those near the plexiglass wall. Also, at the higher air velocity of 3 U_{mf} the tracer concentrations are still closer than when they were mixed at 1.75 U_{mf}.

One final mixing run was carried out where the tracer had been broken up so that the particles were one fourth of their original intact size. The following size distribution was obtained:

-12 +14 : 70% by weight

-14 +20 : 21%

-20 +28 : 9%

The results of this run are graphically summarized in figure 40. With this run, the best results are obtained in achieving near uniformity in concentration when mixed at 3 U_{mf}. However, when the tracer is mixed at 1.75 U_{mf}, there is a separation of tracer concentrations even more pronounced than those at 3 U_{mf}. Whatever the explanation may be for the separation of tracer concentrations at the air velocities below 3 U_{mf}, it is clear that the bed will not become well mixed which is a necessary prerequisite for the use of the discrete space, discrete time model which was to be used for determining the turnover rates and horizontal flow coefficients.

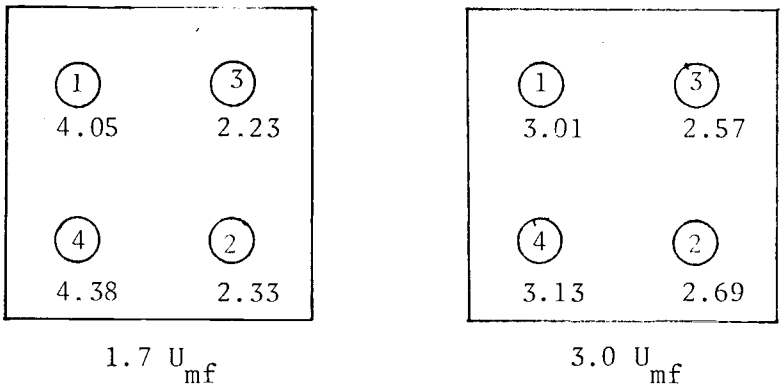

Figure 38 Uncrushed Ferrite
Average Concentrations (lb/ft^3)

Theoretical Mixed Tracer Concentration is 2.59 lb/ft^3

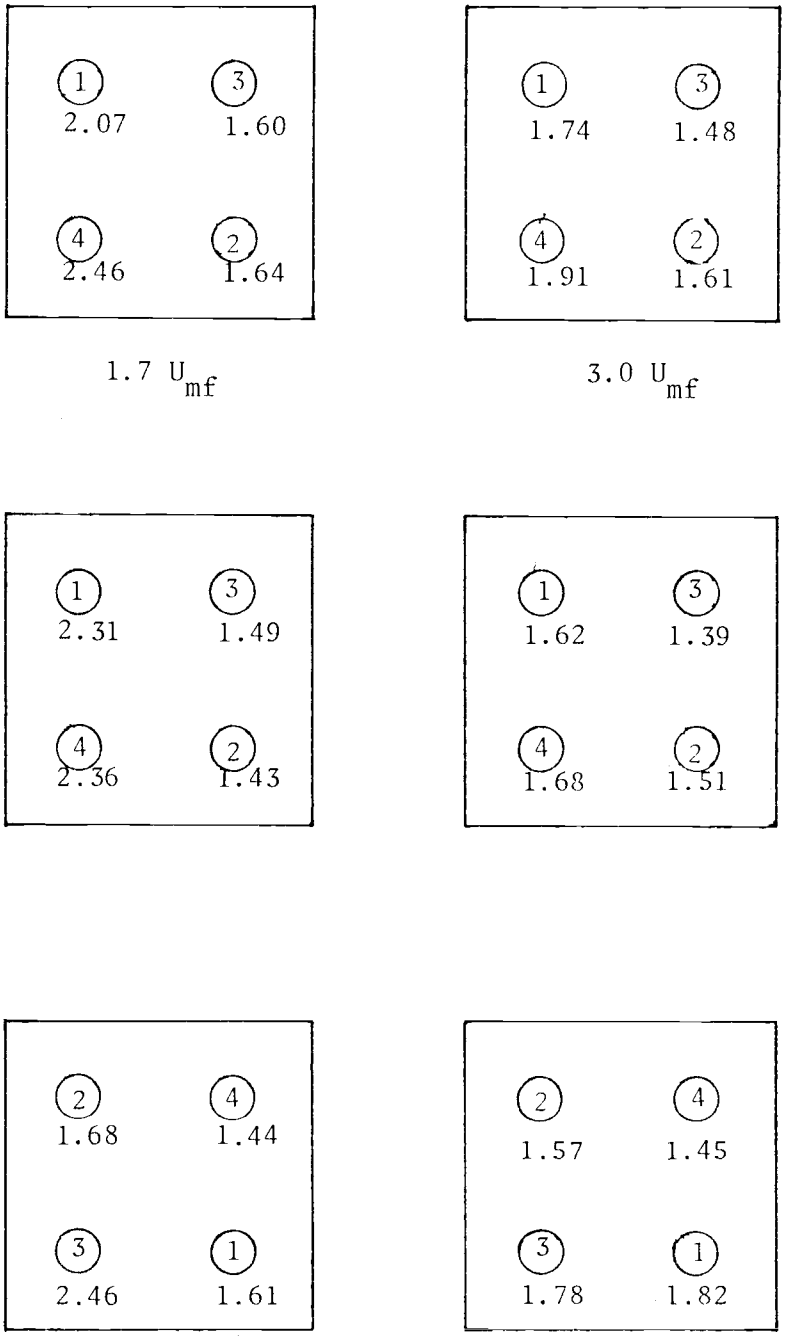

Figure 39 First Crushing of Ferrite
Average concentrations (lb/ft^3)

Theoretical Mixed Tracer Concentration is 1.98 lb/ft^3

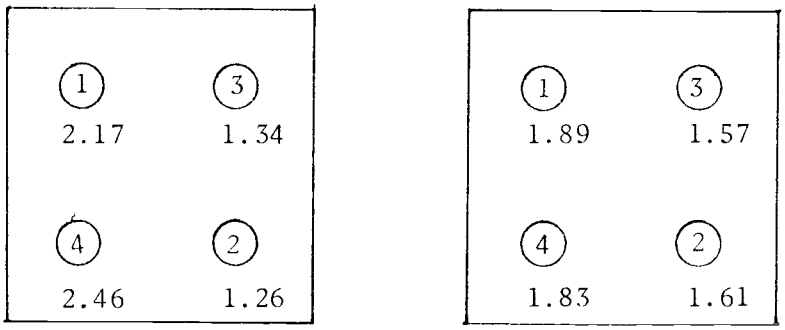

Figure 40 Second Crushing of Ferrite

Average Concentrations (lb/ft^3)

Theoretical Mixed Tracer Concentration is 1.94 lb/ft^3

CONCLUSIONS AND RECOMMENDATIONS

Unfortunately, the poor mixing of tracer in the small fluidized bed made the use of the inductance probe method impossible. The difficulties encountered with the ferrite tracer in this study raise the question of whether any tracer method used in a fluidized bed accurately represents the solids movement in the bed. Based on the results obtained here, the recommended procedure would be to fluidize the solids at air velocities well above U_{mf} such as 2.5 U_{mf} and to use tracer near the same size as that of the other particles in the bed. Between 1-2 U_{mf}, the bed is simply unable to adequately fluidize the whole ferrite core particles. Also, distributor plate design and wall effects in the small bed may be responsible for non-uniform air distribution and solids movement. A larger bed should be more successful in obtaining uniform solids movement.

V. OVERALL CONCLUSIONS AND RECOMMENDATIONS

Even though it wasn't possible to make comparisons between the turnover values obtained using the strain gage probe and the inductance probe, the goals of this thesis project were satisfied. The feasibility of each technique makes each worth further study. The inductance probe method will be used in a bed with a 1 m^2 cross sectional area. The numerous small operating problems which were encountered and solved (and sometimes not solved) helped to debug the prototype circuits and to point out potential problem areas when using the method in the large bed. The strain gage probe method has been shown to be effective in measuring consistent turnover values which are in approximate agreement with the published results of others. This technique still has a good potential for further use in fluidized beds to determine local mass flux values and internal flow patterns in beds. The basic probe design has been shown to work and the recommended redesign should go a long way in alleviating the problems encountered in this study. The idea of a strain sensitive probe should be capable of being extended to use in fluidized combustion boilers where a change of probe materials would be necessary, but the basic concept remains. Mass fluxes could be measured in various regions of the bed with the probe located for example on a heat exchange tube.

BIBLIOGRAPHY

1. J.F. Davidson, AIChE Symp Series, #128,Vol 69, 1973.
2. D. Kunii, O. Levenspiel, Fluidization Engineering, Wiley 1969.
3. J. Verloop, L. DeNie, P. Heertjes, Powd. Tech.,Vol 2,p 32, (1968/69).
4. F.W. Chang, PhD Dissertation, Oregon State University, 1976.
5. J. Highly, D. Merrick, AIChE Symp Series, #116, Vol 67, 1971.
6. W.G. May, Chem. Engr. Prog. Vol 55,pg 49, Dec. 1953.
7. I.M. Razumov, V.V. Manshilin, N.I. Terekhov, O.M. Todes, Khim. Prom., #6, pg 405, 1968.
8. P.N. Rowe, et al, Trans. Inst. Ch. Engrs.,Vol 43,pg 271, 1965.
9. D. Geldart, R.R. Cranfield, Chem. Engr. J., #3, pg 211, 1972.
10. Y. Mori, K. Nakamura, Kagaku Kogaku, Vol 4, #1, 1966.
11. P.N. Rowe, Chem. Engr. Prog., Vol 60, March 1964.
12. I. Hayakawa, Can. J.Ch.E., Vol 42, pg 99, 1964.
13. R.M. Marshek, A. Gomezplata, AIChE. J.,Vol 11, #1, pg 167, 1965.
14. I.M. Razumov, et al, Neftepererabotka i Neftekhim, #7, pg 7, 1970.
15. W. Brötz, Chem. Ing. Tech., Vol 28, pg 165, 1956.
16. I.A. Burovoi, G.I. Svetozarova, Int.Ch.E., Vol 5, #4, Oct. 1965.
17. H.G. Gibson, G.E. Fasching, USBM-IC #8314, pg 42, 1966.

APPENDIX

Table A1 Strain Gage Probe Output for a Tube Filled Bed

Probe	U_o/U_{mf}	Offset (volts)	Unrectified Uncorrected Average (volts)	Rectified + Average (volts)	Rectified - Average (volts)
1	2	+ 0.24	+ 0.18	+ 0.08	- 0.07
2		- 0.27	- 0.36	+ 0.05	- 0.20
3		+ 0.65	+ 0.65	+ 0.17	- 0.04
4		+ 1.00	+ 0.95	+ 0.15	- 0.14
1	1.75	+ 0.20	+ 0.27	+ 0.12	- 0.02
2		- 0.30	- 0.36	+ 0.06	- 0.16
3		+ 0.80	+ 0.80	+ 0.10	- 0.05
4		+ 1.30	+ 1.30	+ 0.12	- 0.20
1	1.5	+ 0.13	+ 0.26	+ 0.20	- 0.00
2		- 0.16	- 0.33	+ 0.02	- 0.20
3		+ 0.70	+ 0.73	+ 0.08	- 0.08
4		+ 1.10	+ 1.20	+ 0.05	- 0.23
1	1.3	+ 0.02	+ 0.04	+ 0.00	- 0.00
2		- 0.50	- 0.45	+ 0.07	- 0.07
3		- 0.50	- 0.50	+ 0.01	- 0.03
4		+ 1.00	+ 1.05	+ 0.08	- 0.10
1	1.75	+ 0.31	+ 0.30	+ 0.05	- 0.07
2		- 0.40	- 0.45	+ 0.05	- 0.07
3		+ 0.70	+ 0.65	+ 0.06	- 0.10
4		+ 1.10	+ 1.25	+ 0.20	- 0.05

Table A2 Turnover Rates For a Tube Filled Bed

Probe	U_o/U_{mf}	+ ⌀ (lb/ft^2-sec)	- ⌀ (lb/ft^2-sec)	Net ⌀ (lb/ft^2-sec)	J_v (lb/ft^2-sec) gm/cm^2-sec
1	2	+ 1.14	- 0.99	+ 0.15	+ 0.78
2		+ 0.71	- 2.84	- 2.13	- 0.78
3		+ 2.41	- 0.57	+ 1.84	avg = 0.78
4		+ 2.13	- 1.99	+ 0.14	(1.52)
1	1.75	+ 1.70	- 0.28	+ 1.42	+ 0.69
2		+ 0.85	- 2.27	- 1.42	- 0.75
3		+ 1.42	- 0.71	+ 0.71	avg = 0.72
4		+ 1.70	- 2.84	- 1.14	(1.47)
1	1.5	+ 2.84	- 0.00	+ 2.84	+ 0.66
2		+ 0.28	- 2.84	- 2.56	- 0.94
3		+ 1.60	- 1.60	0.00	avg = 0.80
4		+ 0.71	- 3.26	- 2.55	(1.64)
1	1.3	+ 0.00	- 0.00	0.00	+ 0.27
2		+ 0.99	- 0.99	0.00	- 0.35
3		+ 0.14	- 0.43	- 0.29	avg = 0.31
4		+ 1.06	- 1.42	- 0.36	(0.63)
1	1.75	+ 0.71	- 0.99	- 0.28	+ 0.62
2	repeat	+ 0.71	- 0.99	- 0.28	- 0.50
3		+ 0.85	- 1.42	- 0.57	avg = 0.56
4		+ 2.85	- 0.71	+ 2.13	(1.15)

Table A3 Strain Gage Probe Output for a Tube Free Bed

Probe	U_o/U_{mf}	Offset (volts)	+ Average (volts)	- Average (volts)
1	2	+ 0.48	+ 0.120	- 0.205
2		- 0.10	+ 0.095	- 0.310
3		+ 0.25	+ 0.110	- 0.210
4		+ 0.80	+ 0.340	- 0.125
1	1.75	- 0.18	+ 0.250	- 0.068
2		- 0.20	+ 0.078	- 0.145
3		+ 0.20	+ 0.115	- 0.177
4		+ 0.75	+ 0.355	- 0.078
1	1.5	- 0.10	+ 0.095	- 0.102
2		- 0.28	+ 0.068	- 0.103
3		+ 0.12	+ 0.118	- 0.095
4		+ 0.68	+ 0.145	- 0.058
1	1.3	- 0.20	+ 0.050	- 0.083
2		- 0.32	+ 0.030	- 0.088
3		+ 0.10	+ 0.050	- 0.107
4		+ 0.64	+ 0.075	- 0.177

Table A4 Turnover Rates for a Tube Free Bed

Probe	U_o/U_{mf}	+ $\dot{\Phi}$ (lb/ft^2-sec)	- $\dot{\Phi}$ (lb/ft^2-sec)	Net $\dot{\Phi}$ (lb/ft^2-sec)	J_v gm/cm^2-sec (lb/ft^2-sec)
1	2	+ 1.70	- 2.91	- 1.21	+ 1.15
2		+ 1.35	- 4.40	- 3.05	- 1.47
3		+ 1.56	- 2.98	- 1.42	avg = 1.31
4		+ 4.82	- 1.77	+ 3.05	(2.68)
1	1.75	+ 3.55	- 0.96	+ 2.59	+ 1.38
2		+ 1.11	- 2.06	- 0.95	- 0.81
3		+ 1.63	- 2.51	- 0.88	avg = 1.10
4		+ 5.04	- 1.11	+ 3.93	(2.25)
1	1.5	+ 1.35	- 1.45	- 0.10	+ 0.74
2		+ 0.96	- 1.46	- 0.50	- 0.62
3		+ 1.67	- 1.35	+ 0.32	avg = 0.68
4		+ 2.06	- 0.82	+ 1.24	(1.39)
1	1.3	+ 0.71	- 1.18	- 0.47	+ 0.36
2		+ 0.43	- 1.25	- 0.82	- 0.79
3		+ 0.71	- 1.52	- 0.81	avg = 0.58
4		+ 1.06	- 2.51	- 1.45	(1.18)